

AD-A094 439

ARMY MISSILE COMMAND REDSTONE ARSENAL AL DIRECTED E--ETC F/G 12/1
DESIGN AND ANALYSIS OF AFOCAL, TWO-MIRROR SYSTEMS FOR ARBITRARY--ETC(U)
OCT 80 W L HALES, D KORSCH

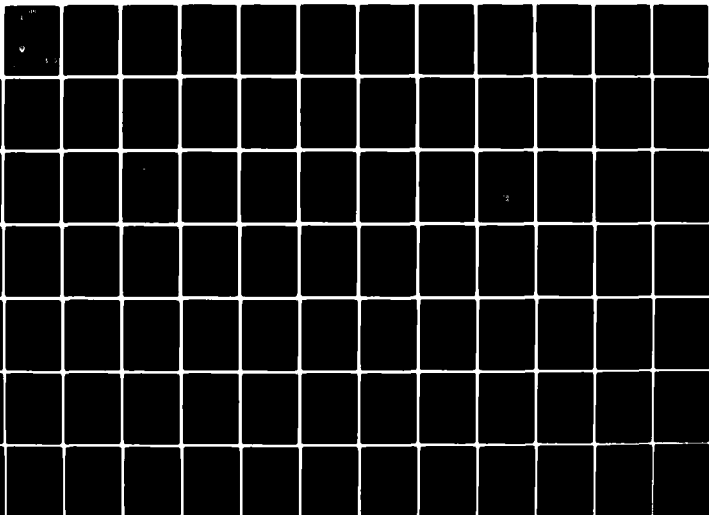
UNCLASSIFIED

DRSMI/RH-81-2-TR

SBIE-AD-E950 075

NL

1 of 1
AD-A094 439



AD A094439

①2 LEVEL III

ade 950 075-

TECHNICAL REPORT RH-81-2

DESIGN AND ANALYSIS OF AFOCAL, TWO-MIRROR
SYSTEMS FOR ARBITRARY INTENSITY TRANSFORMATIONS

Walter LaVaughn Hales
Directed Energy Directorate
US Army Missile Laboratory
and

Dietrich Korsch
TAI Corporation
Huntsville, Alabama

October 1980



U.S. ARMY MISSILE COMMAND

Redstone Arsenal, Alabama 35898

Approved for public release;
distribution unlimited.

DTIC
ELECTE
S FEB 3 1981 D
B

DBC FILE COPY

SMI FORM 1021, 1 JUL 79 PREVIOUS EDITION IS OBSOLETE

81 2 02 178

DISPOSITION INSTRUCTIONS

**DESTROY THIS REPORT WHEN IT IS NO LONGER NEEDED. DO NOT
RETURN IT TO THE ORIGINATOR.**

DISCLAIMER

**THE FINDINGS IN THIS REPORT ARE NOT TO BE CONSTRUED AS AN
OFFICIAL DEPARTMENT OF THE ARMY POSITION UNLESS SO DESIGNATED BY OTHER AUTHORIZED DOCUMENTS.**

TRADE NAMES

**USE OF TRADE NAMES OR MANUFACTURERS IN THIS REPORT DOES
NOT CONSTITUTE AN OFFICIAL INDORSEMENT OR APPROVAL OF
THE USE OF SUCH COMMERCIAL HARDWARE OR SOFTWARE.**

UNCLASSIFIED

SECURITY CLASSIFICATION OF THIS PAGE (When Data Entered)

REPORT DOCUMENTATION PAGE		READ INSTRUCTIONS BEFORE COMPLETING FORM
1. REPORT NUMBER Technical Report RH-81-2	2. GOVT ACCESSION NO. AD-A094 439	3. RECIPIENT'S CATALOG NUMBER
4. TITLE (and Subtitle) DESIGN AND ANALYSIS OF AFocal, TWO-MIRROR SYSTEMS FOR ARBITRARY INTENSITY TRANSFORMATIONS		5. TYPE OF REPORT & PERIOD COVERED Technical Report
7. AUTHOR(s) Walter LaVaughn Hales (Directed Energy Directorate) Dietrich Korsch (TAI Corporation)		6. PERFORMING ORG. REPORT NUMBER
9. PERFORMING ORGANIZATION NAME AND ADDRESS Commander, US Army Missile Command Attn: DRSMI-RH Redstone Arsenal, AL 35898		8. CONTRACT OR GRANT NUMBER(s)
11. CONTROLLING OFFICE NAME AND ADDRESS Commander, US Army Missile Command Attn: DRSMI-RPT Redstone Arsenal, AL 35898		10. PROGRAM ELEMENT, PROJECT, TASK AREA & WORK UNIT NUMBERS
14. MONITORING AGENCY NAME & ADDRESS (if different from Controlling Office)		12. REPORT DATE October 1980
		13. NUMBER OF PAGES 88
		15. SECURITY CLASS. (of this report) Unclassified
		15a. DECLASSIFICATION/DOWNGRADING SCHEDULE
16. DISTRIBUTION STATEMENT (of this Report) Approved for public release; distribution unlimited.		
17. DISTRIBUTION STATEMENT (of the abstract entered in Block 20, if different from Report)		
18. SUPPLEMENTARY NOTES		
19. KEY WORDS (Continue on reverse side if necessary and identify by block number) Reflecting systems Intensity modification Telescopes Toroidal reflectors Beam expanders		
20. ABSTRACT (Continue on reverse side if necessary and identify by block number) Generalized surface equations are developed for reflexicon and waxicon systems, which allow arbitrary control of the intensity profile of the exit beam. These equations assume axial symmetry of the intensity transformation function. Both the reflexicon and waxicon systems are analyzed numerically to determine the sensitivity of the aberrations to system misalignment and system design parameters. Design recommendations are made for minimizing the sensitivity of the systems to misalignment.		

DD FORM 1 JAN 73 1473

EDITION OF 1 NOV 65 IS OBSOLETE

UNCLASSIFIED

SECURITY CLASSIFICATION OF THIS PAGE (When Data Entered)

ACKNOWLEDGMENTS

The authors wish to thank Mr. Jerry D. Smith, DMIS, for his valuable assistance in computer programming, and Dr. Thomas G. Roberts, MICOM, and Dr. Charles L. Wyman, NASA, for their helpful comments and criticism.

Accession For	
NTIS GRA&I	<input checked="" type="checkbox"/>
DTIC TAB	<input type="checkbox"/>
Unannounced	<input type="checkbox"/>
Justification	
By	
Distribution/	
Availability Codes	
Dist	Avail and/or Special
A	

TABLE OF CONTENTS

	Page
Chapter I. INTRODUCTION	5
Chapter II. REFLAXICON SYSTEMS.	11
A. Reflaxicon Surface Equations.	11
B. Constant Ray-Height Transformation.	14
C. Parabolic Reflaxicons	18
D. Beam-Shape Distortion	19
E. Intensity Transformation.	21
1. Parabolic Reflaxicons	28
2. Constant-Intensity Reflaxicons.	30
Chapter III. WAXICON SYSTEMS.	36
A. Generalized Surface Equations	36
B. Intensity Transformation.	39
C. Constant-Intensity Waxicons	42
Chapter IV. PERFORMANCE ANALYSIS.	49
A. Ray-Tracing Procedures.	49
B. Reflaxicon Systems.	50
1. Mirror Tilt	52
2. Decentering	58
3. Despacing	63
4. Off-Axis Angle.	64
5. Inside Radius of Annular Beam	65
6. Intensity Transformation.	65
7. Statistical Analysis.	66
C. Waxicon Systems	78
1. Decentering	79
2. Tilt in the Waxicon	80
3. Off-Axis Angle.	86
Chapter V. CONCLUSIONS.	88
SELECTED BIBLIOGRAPHY.	90

LIST OF FIGURES

	Page
Figure 1. Typical reflaxicon (a) and waxicon (b) systems	6
Figure 2. Focusing properties of conic sections.	7
Figure 3. Two-mirror afocal systems using confocal paraboloids.	9
Figure 4. Eccentric-pupil systems using confocal paraboloids.	10
Figure 5. Diagram of reflaxicon system	12
Figure 6. Parabolic reflaxicon	17
Figure 7. Transformation of beam-shape in a parabolic reflaxicon with an eccentric pupil	20
Figure 8. Grazing-incidence (a) and normal-incidence (b) reflaxicons ($I = 0.1$, $b = 1.5$)	27
Figure 9. Radial energy distribution of parabolic reflaxicon, compared with equivalent constant intensity distribution	30
Figure 10. Forward-reflecting constant-intensity reflaxicon. . .	33
Figure 11. Near-normal-incidence constant-intensity reflaxicon.	33
Figure 12. Constant-intensity reflaxicon giving unit beam- intensity transformation.	34
Figure 13. Diagram of waxicon system	37
Figure 14. Waxicon with near-grazing-incidence on the inner mirror.	45
Figure 15. Waxicon with nearly equal angles of incidence of both mirrors	46

	Page
Figure 16. Waxicon with near-grazing-incidence on the outer mirror	47
Figure 17. Beam decollimation produced by a constant tilt of 0.1 mrad on the outer mirror, as a function of shape factor.	52
Figure 18. Centroid shift produced by constant tilt of 0.1 mrad on the outer mirror, as a function of the shape factor.	54
Figure 19. Beam decollimation versus tilt of outer mirror . . .	55
Figure 20. Sensitivity of decollimation to pivot-point of outer-mirror tilt (tilt angle = 0.1 mrad).	56
Figure 21. Nomogram relating beam decollimation, shape factor, and tilt of outer mirror	57
Figure 22. Beam decollimation versus decenter of outer mirror .	59
Figure 23. Beam decollimation versus shape factor for constant decenter of 0.002 cylindrical beam diameters at the outer mirror	60
Figure 24. Nomogram relating beam-decollimation, shape factor, and decentering of outer mirror.	61
Figure 25. Centroid shift versus shape factor for constant decenter of 0.002 cylindrical beam diameters at the outer mirror.	62
Figure 26. Beam decollimation versus despadding of mirrors . . .	63
Figure 27. Beam decollimation versus off-axis angle of incident cylindrical beam	64
Figure 28. Beam decollimation versus inside radius of annular beam for constant tilt of 0.1 mrad at outer mirror	66
Figure 29. Beam decollimation versus inside radius of annular beam for constant decenter of 0.002 cylindrical beam diameters at outer mirror	67
Figure 30. Beam decollimation versus intensity transformation for constant tilt of 0.1 mrad at outer mirror. . . .	68

	Page
Figure 31. Beam decollimation versus intensity transformation for constant decenter of 0.002 cylindrical beam diameters at outer mirror	69
Figure 32. Statistical beam decollimation versus shape factor for tilt limits of 0.1 mrad and shift limits of 0.001 cylindrical beam diameter with standard deviations.	70
Figure 33. Decollimation distribution, $k = 0.1$	71
Figure 34. Decollimation distribution, $k = 0.5$	72
Figure 35. Decollimation distribution, $k = 1$	73
Figure 36. Decollimation distribution, $k = 2$	74
Figure 37. Decollimation distribution, $k = 3$	75
Figure 38. Decollimation distribution, $k = 4$	76
Figure 39. Decollimation distribution, $k = 5$	77
Figure 40. Beam decollimation versus shape factor for constant decenter of 0.001 cylindrical beam diameters at outer mirror	80
Figure 41. Beam decollimation versus decenter of outer mirror for constant C	81
Figure 42. Nomogram relating beam decollimation, shape factor, and decentering of outer mirror	82
Figure 43. Beam decollimation versus shape factor for constant outer mirror tilt of 0.1 mrad.	83
Figure 44. Beam decollimation versus tilt of outer mirror. . . .	84
Figure 45. Nomogram relating beam decollimation, shape factor, and tilt angle.	85
Figure 46. Beam decollimation versus off-axis angle of incident cylindrical beam	86

Chapter I. INTRODUCTION

Axicon-type optical systems have received increased attention in recent years because of the peculiar problems associated with handling high-power laser beams. In high-power laser systems, any backscatter, or retroflection of the beam into the laser system can be disastrous. Also, many high-power lasers have annular output beams, which need to be transformed into cylindrical beams, with no hole in the center, for good propagation characteristics in the atmosphere.

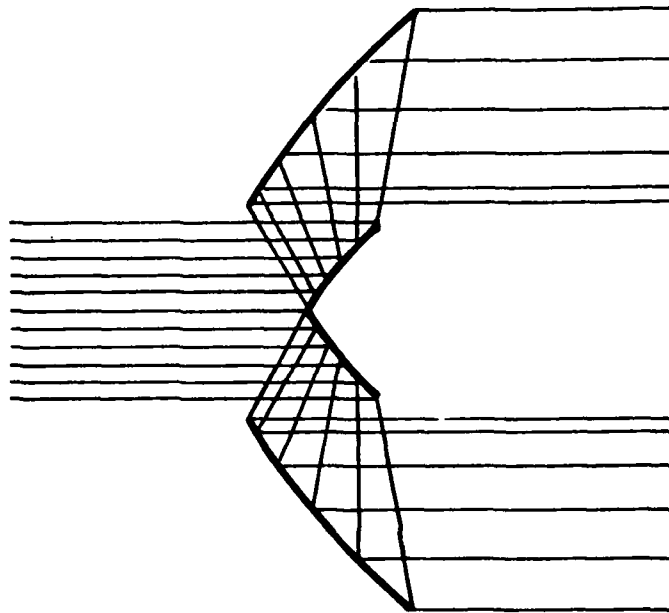
The sharply pointed mirrors, characteristic of reflaxicon and waxicon systems, are ideally suited for handling these problems. These systems are illustrated in Figure 1.

Pointed mirrors are almost impossible to produce by classical grinding and polishing techniques, but can be made very easily on a single-point diamond lathe.

Because these systems have only recently become practical, very little theoretical work has been done on them. It is the purpose of this paper to develop generalized surface-equations which will permit arbitrary transformation of the radial intensity distribution of the laser beam, and to determine the relative sensitivities of such systems to various types of misalignment. Guidelines will be established for optimizing the performance of the systems.

Nonlinear reflecting systems have traditionally been based on the focusing properties of conic sections of revolution. As is well known,

(a)



(b)

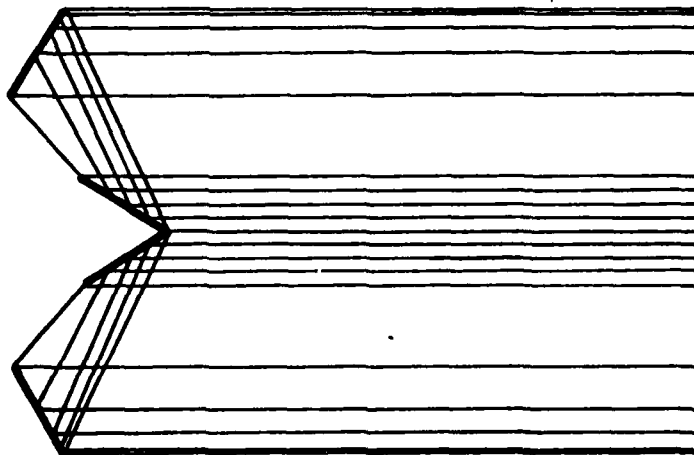


Figure 1. Typical reflexicon (a) and waxicon (b) systems.

conic sections of revolution have two foci and, have the property that all rays originating at either focus, and intercepting the surface, will be reflected to the conjugate focus. The optical path-length (OPL) traversed by a ray as it goes from one focus to the surface, then to the conjugate focus, is invariant, i.e., spherical aberration is absent. Figure 2 illustrates the basic surfaces and their foci. In the case of a sphere, the conjugate foci are degenerate; in the case of a paraboloid, one focus is at infinity.

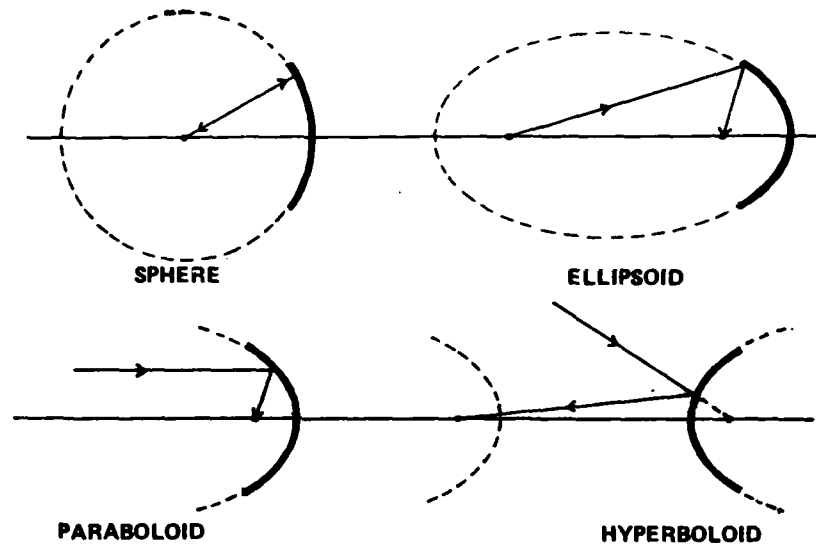


Figure 2. Focusing properties of conic sections.

The conic surfaces may be used in any combination to form compound systems free of spherical aberration, so long as the corresponding foci for consecutive surfaces are coincident. Surfaces with such coincident foci are said to be confocal.

For the purpose of this study, only the systems which transform a bundle of rays, parallel to the axis, into another bundle parallel to

the axis will be considered. Here, the conjugate foci of the system are at \pm infinity. Such systems are said to be afocal. Further, this study will be restricted to two-mirror systems.

The classical two-mirror, afocal system consists of two confocal paraboloids. The input and output beams may propagate in the same direction, or in opposite directions, as shown in Figure 3. For that matter, the axes of the two paraboloids may be oriented in any conceivable direction, relative to one another, but for the purposes of this study, they are colinear.

Both systems shown in Figure 3 have a common fault that restricts their application in laser systems. The paraxial rays of the input beam are reflected back toward the laser and will re-enter the laser and upset the mode control or may damage the front of the laser hardware. Such systems may, however, prove useful when used with an eccentric aperture, or when used with a laser having an annular output beam. Such systems are shown in Figure 4.

The systems investigated in this paper will be those capable of transforming a cylindrical input beam into an annular output beam, or vice-versa, without obscuring or misdirecting any of the input rays. Further, we shall seek a solution which allows arbitrary control of the intensity distribution within the annular output beam. These systems are of importance in optimizing the beam propagation through the atmosphere, and in increasing the efficiency of the beam in cutting and welding operations. They would commonly be used in conjunction with other, more traditional, optical systems in a beam control system.

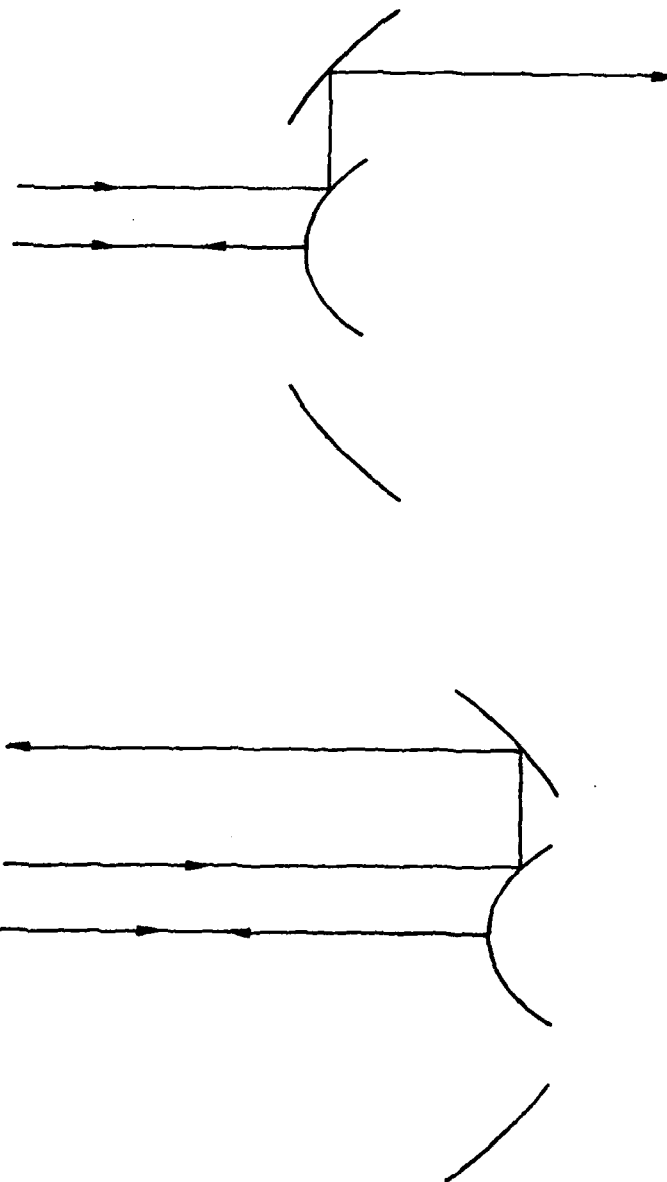


Figure 3. Two-mirror afocal systems using confocal paraboloids.

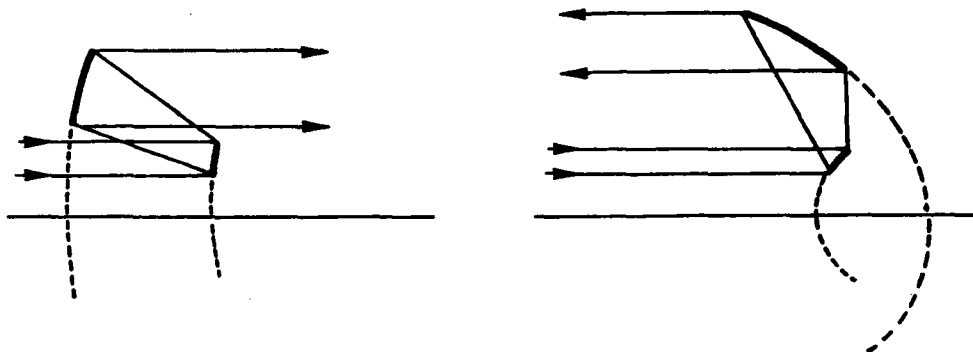


Figure 4. Eccentric-pupil systems using confocal paraboloids.

These systems may also be applied as cavity mirrors in lasers, and in transforming annular laser beams into cylindrical beams in some master oscillator-amplifier systems.

Chapter II. REFLAXICON SYSTEMS

A. Reflaxicon Surface Equations

The surface equations for an afocal reflaxicon will now be developed allowing an arbitrary ray-height transformation. Two conditions shall be imposed:

a) Any entrance ray, parallel to the axis, must emerge parallel to the axis, i.e., the system must be afocal.

b) The optical path-length between the entrance plane, z_0 , and the exit plane, z_3 , must be constant.

For convenience, the equations will be developed in cylindrical coordinates.

If the ray-intercepts of the inner and outer mirrors are designated by (r_1, z_1) and (r_2, z_2) , respectively, Figure 5 shows that the OPL of a ray between z_0 and z_3 is given by

$$\text{OPL} = z_1 - z_0 + \sqrt{(z_2 - z_1)^2 + (r_2 - r_1)^2} + z_3 - z_2 = L \quad (1)$$

Then,

$$\sqrt{(z_2 - z_1)^2 + (r_2 - r_1)^2} = L - z_1 + z_0 - z_3 + z_2 = k - z_1 + z_2, \quad (2)$$

where $k = L + z_0 - z_3$ is a constant, and represents the OPL added by the system as the ray passes from z_0 to z_3 . Squaring Equation (2), the following is obtained:

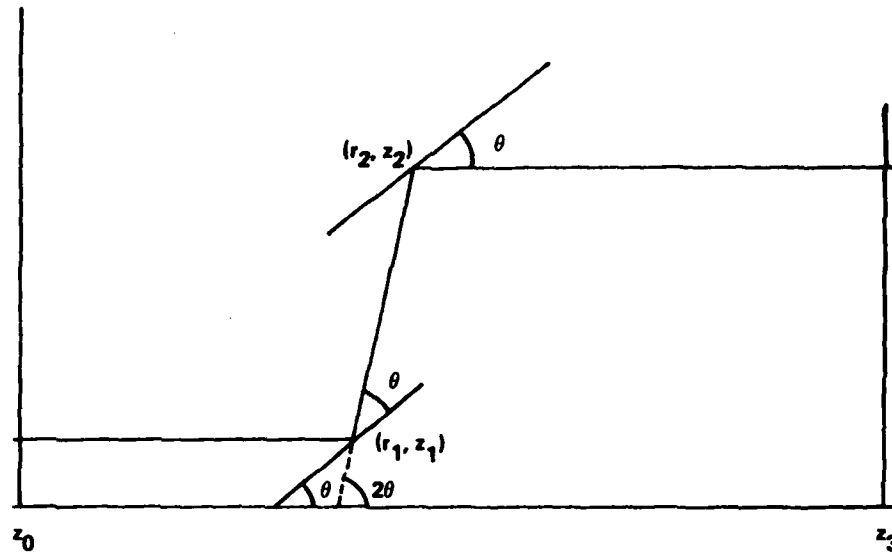


Figure 5. Diagram of reflexicon system.

$$(z_2 - z_1)^2 + (r_2 - r_1)^2 = k^2 + 2k(z_2 - z_1) + (z_2 - z_1)^2, \quad (3)$$

or,

$$(r_2 - r_1)^2 = k^2 - 2k(z_2 - z_1). \quad (4)$$

Noting in Figure 5 that

$$\tan 2\theta = \frac{r_2 - r_1}{z_2 - z_1}, \quad (5)$$

and dividing Equation (4) by $r_2 - r_1$,

$$r_2 - r_1 = \frac{k^2}{r_2 - r_1} + \frac{2k}{\tan 2\theta}. \quad (6)$$

Thus,

$$\tan 2\theta = \frac{2k(r_2 - r_1)}{(r_2 - r_1)^2 - k^2}. \quad (7)$$

This provides a system equation for the condition of constant path-length.

Applying the half-angle formula for the tangent function,

$$\tan \theta = \frac{-1 \pm \sqrt{1 + \tan^2 2\theta}}{\tan 2\theta}, \quad (8)$$

we see that:

$$\tan \theta = \frac{-1 \pm \sqrt{1 + \left[\frac{2k(r_2 - r_1)}{(r_2 - r_1)^2 - k^2} \right]^2}}{\frac{2k(r_2 - r_1)}{(r_2 - r_1)^2 - k^2}} \quad (9)$$

which, after some algebra, yields

$$\tan \theta = \frac{-(r_2 - r_1)^2 + k^2 \pm [(r_2 - r_1)^2 + k^2]}{2k(r_2 - r_1)} \quad (10)$$

Taking the positive value of the dual sign,

$$\tan \theta = \frac{k}{r_2 - r_1}. \quad (11)$$

It is obvious from simple geometrical considerations, that for an afocal system,

$$\tan \theta = \frac{dr_1}{dz_1} = \frac{dr_2}{dz_2}. \quad (12)$$

By integrating this expression, we have for the inner mirror,

$$k \int dz_1 = \int (r_2 - r_1) dr_1 \quad (13)$$

or

$$z_1 = \frac{\int r_2 dr_1 - \frac{1}{2} r_1^2 + C}{k}, \quad (14)$$

where C is an arbitrary constant of integration.

Applying the afocal condition to the outer mirror,

$$k \int dz_2 = \int (r_2 - r_1) dr_2, \quad (15)$$

or

$$z_2 = \frac{\frac{1}{2} r_2^2 - \int r_1 dr_2 + C'}{k} = \frac{\frac{1}{2} r_2^2 - r_1 r_2 + \int r_2 dr_1 + C'}{k}. \quad (16)$$

Now the constants of integration, C and C', must be related by requiring that Equations (14) and (16) satisfy the constant path-length condition, thereby eliminating spherical aberration. The simultaneous solution of Equations (4), (14), and (16) yields

$$\begin{aligned} r_2^2 - 2r_1 r_2 + r_1^2 = k^2 + 2\left(\frac{1}{2} r_2^2 - r_1 r_2 \right. \\ \left. + \int r_2 dr_1 + C' - \int r_2 dr_1 + \frac{1}{2} r_1^2 - C\right) \end{aligned} \quad (17)$$

or,

$$k^2 + 2(C' - C) = 0 \quad (18)$$

and

$$C' = -\frac{k^2}{2} + C. \quad (19)$$

Substituting this into Equation (16),

$$z_2 = \frac{\frac{1}{2} r_2^2 - r_1 r_2 + \int r_2 dr_1 - \frac{k^2}{2} + C}{k}. \quad (20)$$

Equations (14) and (20) are the surface equations for the inner and outer mirrors, respectively, as functions of the radial distance between a ray and the axis.

B. Constant Ray-Height Transformation

Since (r_1, z_1) and (r_2, z_2) are the corresponding ray intercepts at the inner and outer mirrors, respectively, Equations (14) and (20)

may be rewritten eliminating r_2 , by introducing a ray-height transformation function defined by

$$M(r_1) = \frac{r_2}{r_1} \quad (21)$$

$M(r_1)$ is simply the magnification of the input ray-height produced by the optical system. Substituting this transformation into Equations (14) and (20), the following is obtained:

$$z_1 = \frac{\int r_1 M(r_1) dr_1 - \frac{1}{2} r_1^2 + C}{k} \quad (22)$$

$$z_2 = \frac{\frac{1}{2} [r_1 M(r_1)]^2 - r_1^2 M(r_1) + \int r_1 M(r_1) dr_1 - \frac{k^2}{2} + C}{k} \quad (23)$$

and,

$$r_2 = r_1 M(r_1) \quad (24)$$

These forms of the surface equations are very convenient when performing numerical calculations.

Here, it should be noted that if the ray-height transformation, $M(r_1)$, is constant for all r_1 , i.e., $M(r_1) = M$, the surface equations become

$$z_1 = \frac{\frac{M}{2} r_1^2 - \frac{1}{2} r_1^2 + C}{k} = \frac{M-1}{2k} r_1^2 + \frac{C}{k} \quad (25)$$

and

$$\begin{aligned} z_2 &= \frac{\frac{1}{2} r_2^2 + \frac{M}{2} r_1^2 - \frac{r_2^2}{M} - \frac{k^2}{2} + C}{k} = \frac{\frac{1}{2} r_2^2 + \frac{r_2^2}{2M} - \frac{r_2^2}{M} - \frac{k^2}{2} + C}{k} \\ &= \frac{M-1}{2kM} r_2^2 + \frac{2C - k^2}{2k} = \frac{M(M-1)}{2k} r_1^2 + \frac{2C - k^2}{2k} \end{aligned} \quad (26)$$

Thus, both mirrors are simple paraboloids, with the inner and outer mirrors having their vertices at $z_{v1} = C/k$ and $z_{v2} = (2C - k^2)/2k$, respectively.

Recalling the parabolic equation

$$z = \frac{1}{4F} r^2 + a \quad (27)$$

which represents a paraboloid (in cylindrical coordinates) with a focal length, F , and the vertex at $z = a$, it can be seen from Equations (25) and (26), that

$$\frac{M - 1}{2k} = \frac{1}{4F_1} \quad (28)$$

and

$$\frac{M - 1}{2kM} = \frac{1}{4F_2} \quad (29)$$

where F_1 and F_2 are the focal lengths of the inner and outer mirrors, respectively. Thus,

$$F_1 = \frac{k}{2(M - 1)} \quad , \quad (30)$$

$$F_2 = \frac{kM}{2(M - 1)} \quad , \quad (31)$$

and

$$\frac{F_2}{F_1} = M \quad . \quad (32)$$

The ray height magnification is given by the ratio of the focal lengths of the two paraboloids. The locations of the foci on the z -axis are

$$z_{F_1} = a + F_1 = \frac{C}{k} + \frac{k}{2(M - 1)} \quad (33)$$

and

$$z_{F_2} = a + F_2 = \frac{C}{k} + \frac{k}{2(M - 1)} \quad . \quad (34)$$

Thus, $z_{F_1} = z_{F_2}$, and the mirrors are confocal.

The system with constant M has the disadvantage of retroreflection of the paraxial rays, but may be used with annular input-beams, or with cylindrical beams in an eccentric-pupil arrangement. It is, in fact, the only afocal system which preserves the beam shape, when used with an eccentric beam.

Since M is constant, it also gives a constant intensity transformation. The intensity of the output beam is $1/M^2$ times the intensity of the input beam.

The problem of the retroreflection of the paraxial rays can be alleviated by displacing the axis of revolution of the parabolas from the geometrical axis. This is illustrated in Figure 6.

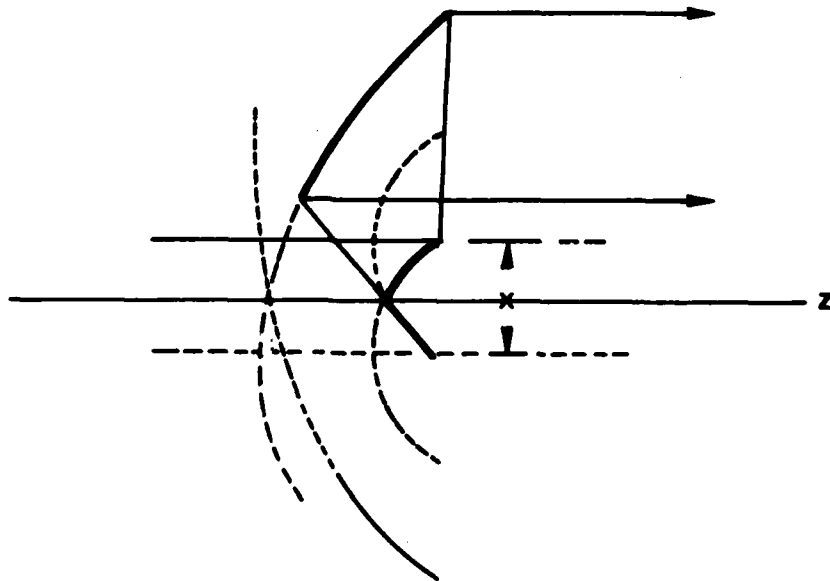


Figure 6. Parabolic reflaxicon.

C. Parabolic Reflaxicons

In this system, the geometrical axis of the parabolas is changed from a line into a cylinder, and the focal points become focal circles. The mirror surfaces are now toroidal. With a sufficient displacement of the geometrical axis from the axis of symmetry, or optical axis, all rays impinging on the inner mirror will be reflected to the outer mirror and will continue out of the system without obscuration by the inner mirror.

Referring again to Figure 6, it can be seen that the two-dimensional meridional sections of the mirrors are exactly the same as those of the mirrors in the simple parabolic case, except that the curves are translated in the r -direction. Since the two-dimensional equations in cartesian coordinates are the same as the three-dimensional equations in cylindrical coordinates, the surface equations of the mirrors may easily be written as

$$z_1 = \frac{M-1}{2k} (r_1 + h)^2 + \frac{C}{k} \quad (37)$$

and

$$z_2 = \frac{M-1}{2kM} (r_2 + h)^2 + \frac{2C - k^2}{2k} \quad (38)$$

where h is the distance the geometrical axis is displaced from the optical axis and is taken as a positive quantity. M is the constant ratio

$$M = \frac{F_2}{F_1} = \frac{r_2 + h}{r_1 + h} \quad (39)$$

This system offers two serious disadvantages. One will notice that an arbitrarily small annulus of rays about the optical axis will be expanded into an annulus at the inside edge of the outer mirror. This effects an arbitrarily large radial, and consequently, large area magnification, thereby reducing the intensity in the output beam to near zero. For good, long-range atmospheric propagation, it is desirable to have the maximum intensity at the inside of the beam. Also, if one uses the system in reverse with a large annular input beam, and a small cylindrical output beam, the relatively intense inside edge of the annular beam is reduced to an arbitrarily small diameter, and the intensity becomes arbitrarily large. Here, of course, diffraction effects are neglected. The use of the system in this mode with a high-energy laser would result in the destruction of the axial region of the mirror.

The second disadvantage is that the system is usually unsuitable for use with an eccentric entrance pupil, to allow a solid (non-annular) beam to be transformed into another solid beam. This is also caused by the variable radial magnification in the system. It has already been shown that the beam shape can be preserved only in the case of constant ray-height magnification.

D. Beam Shape Distortion

Figure 7 presents the effect of beam-shape distortion in the parabolic reflaxicon system. Here, the viewer is looking down the optical axis at the profiles of the input and output beams. Within

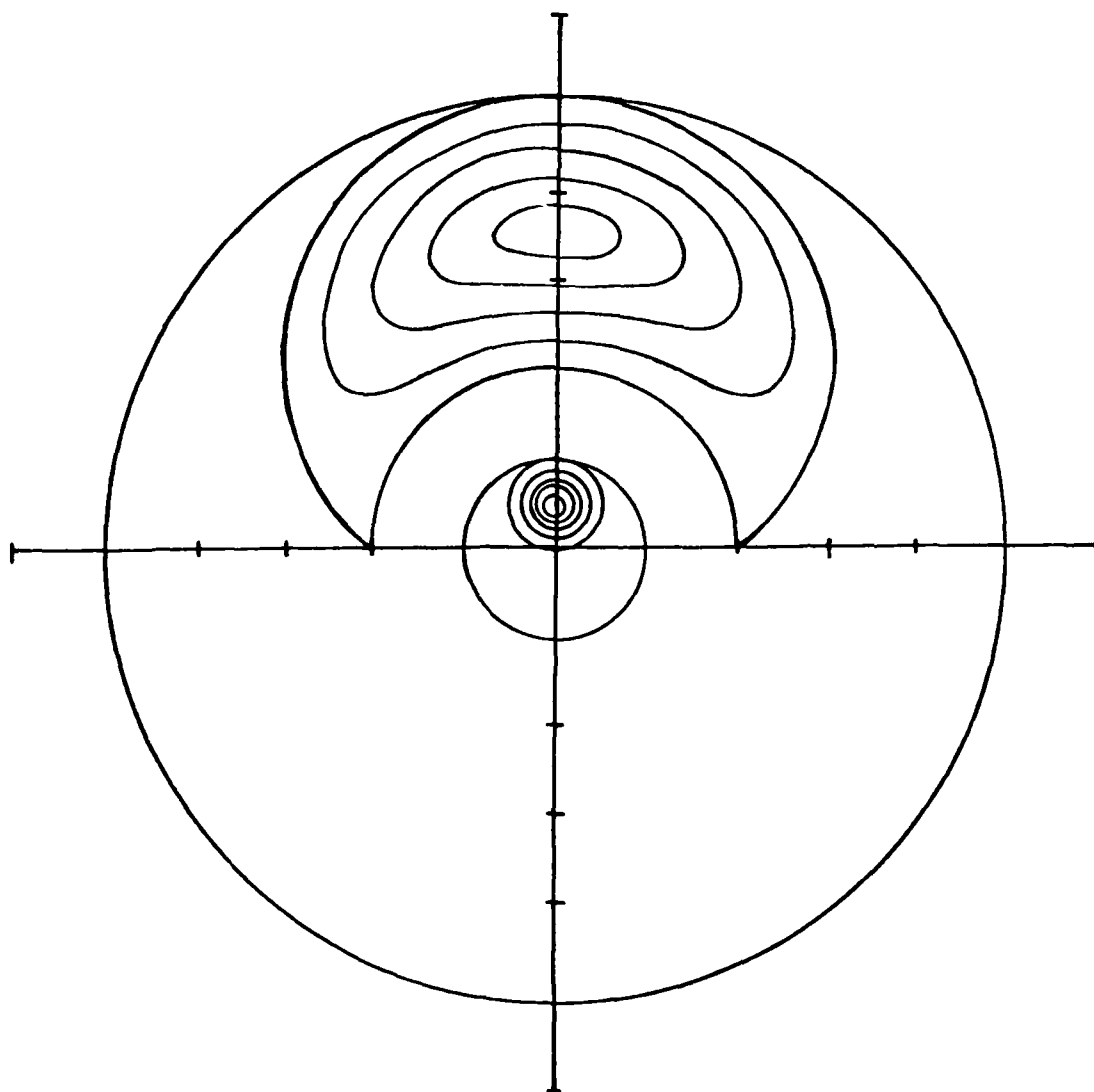


Figure 7. Transformation of beam shape in a parabolic reflaxicon with an eccentric pupil.

the boundary of the inner mirror, a bulls-eye pattern can be seen representing the boundaries of several eccentric, cylindrical input beams. They are all centered about an input ray-height of 0.5 units. The inner mirror is 2.0 units in diameter, the displacement of the parabolic axis, h , is 1 unit, $M^* = 3$, and the outer mirror is 10 units in diameter. The large, distorted ovals are the boundaries of the output-beams, corresponding to the cylindrical input-beams. It can be seen that a very small input beam, well-removed from the optical axis, may produce a usable, elliptical output-beam. The suitability of such a beam would depend entirely on the application.

Since the reflaxicon would usually be used in critical applications requiring precise control of the intensity distribution within the beam, attention will now be directed to the beam intensity transformation function.

E. Intensity Transformation

If the area of a beam, or element of a beam, is magnified by some factor, the intensity will change as the inverse of the area magnification. One's first inclination may be to say that if the linear magnification is M , the area magnification M^2 , and the intensity will be changed by M^{-2} . However, this is true only for a constant magnification. It has been seen that in an afocal reflaxicon, the magnification of the ray-heights is constant only if the mirrors are simple paraboloids, with their geometrical axes colinear with the axis of symmetry, or optical axis of the system. If the geometrical axes of the

surfaces are displaced from the axis of symmetry of the system, the ray-height magnification is variable. The area magnification and the intensity transformation will now be examined when the linear magnification is variable.

As before, the ray-height transformation is defined by

$$M(r_1) = \frac{r_2}{r_1} .$$

It is now assumed that an input annulus has an inside radius, r_1 , and a width, dr_1 . This annulus will be transformed into an output annulus having an inside radius of r_2 , and a width of dr_2 . The area of the input annulus is given by

$$A_1 = 2\pi r_1 dr_1 \quad (40)$$

and that of the output annulus is

$$A_2 = 2\pi r_2 dr_2 . \quad (41)$$

Since

$$\begin{aligned} r_2 &= r_1 M(r_1) , \\ \frac{dr_2}{dr_1} &= M(r_1) + r_1 \frac{dM(r_1)}{dr_1} . \end{aligned} \quad (42)$$

Equation (41) now becomes

$$A_2 = 2\pi r_1 M(r_1) \left[M(r_1) + r_1 \frac{dM(r_1)}{dr_1} \right] dr_1 \quad (43)$$

and the area magnification is

$$\frac{A_2}{A_1} = [M(r_1)]^2 + r_1 M(r_1) \frac{dM(r_1)}{dr_1} . \quad (44)$$

Now, the intensity transformation function $\vartheta(r_1)$ is defined by the relationship

$$\vartheta(r_1) = \frac{I_o(r_2)}{I_i(r_1)}, \quad (45)$$

where $I_i(r_1)$ and $I_o(r_2)$ are the intensities of the input and output beams, respectively. Since the intensity of the output beam is inversely proportional to the area magnification,

$$\vartheta(r_1) = \frac{A_1}{A_2} = \frac{1}{[M(r_1)]^2 + r_1 M(r_1) \frac{dM(r_1)}{dr_1}}. \quad (46)$$

For a given intensity transformation, $\vartheta(r_1)$, the required ray-height magnification, $M(r_1)$, can be found from the differential equation

$$\frac{dM(r_1)}{dr_1} r_1 M(r_1) + [M(r_1)]^2 - \frac{1}{\vartheta(r_1)} = 0. \quad (47)$$

Rearranging terms,

$$\frac{dM(r_1)}{dr_1} + \frac{M(r_1)}{r_1} = \frac{1}{\vartheta(r_1) r_1 M(r_1)}. \quad (48)$$

This is in the form of Bernoulli's equation,

$$\frac{dy}{dx} + P(x)y = Q(x)y^n \quad (49)$$

where

$$\begin{aligned} \frac{dy}{dx} &= \frac{dM(r_1)}{dr_1} & Q(x) &= \frac{1}{\vartheta(r_1) r_1} \\ x &= r_1 & y &= M(r_1) \\ P(x) &= \frac{1}{r_1} & n &= -1 \end{aligned}$$

Letting

$$v = y^{1-n} = y^2 ,$$

and

$$\frac{dv}{dx} = 2y \frac{dy}{dx} ,$$

Equation (49) reduces to

$$\frac{1}{2} \frac{dv}{dx} + P(x)v = Q(x) \quad (50)$$

or

$$\frac{dv}{dx} + 2P(x)v = 2Q(x) . \quad (51)$$

This linear equation may be solved by choosing the integrating factor

$$\mu = e^{2\int P(x)dx} . \quad (52)$$

The solution is then

$$ve^{2\int P(x)dx} = 2\int Q(x)e^{2\int P(x)dx}dx + b . \quad (53)$$

Translating this back into the original variables, and noting that

$$2P(x)dx = 2\int \frac{1}{r_1} dr_1 = \ln r_1^2 , \quad (54)$$

$$[M(r_1)r_1]^2 = 2\int \frac{1}{r_1\phi(r_1)} r_1^2 dr_1 + b = 2\int \frac{r_1}{\phi(r_1)} dr_1 + b = r_2^2 . \quad (55)$$

Recalling the surface equation for the inner mirror,

$$z_1 = \frac{\int r_2 dr_1 - \frac{1}{2} r_1^2 + C}{k}$$

$$z_1 = \frac{\int \left[2 \int \frac{r_1}{\phi(r_1)} dr_1 + b \right]^{\frac{1}{2}} dr_1 - \frac{1}{2} r_1^2 + C}{k} . \quad (56)$$

Likewise, the surface equation for the outer mirror becomes

$$\begin{aligned}
 z_2 &= \frac{\frac{1}{2} r_2^2 - r_1 r_2 + \int r_2 dr_1 - \frac{k^2}{2} + C}{k} \\
 z_2 &= \frac{\int \frac{r_1}{\vartheta(r_1)} dr_1 + \frac{b}{2} - r_1 \left[2 \int \frac{r_1}{\vartheta(r_1)} dr_1 + b \right]^{\frac{1}{2}}}{k} \\
 &+ \frac{\int \left[2 \int \frac{r_1}{\vartheta(r_1)} dr_1 + b \right]^{\frac{1}{2}} dr_1 - \frac{k^2}{2} + C}{k} .
 \end{aligned} \tag{57}$$

These surface equations appear rather formidable, but are entirely practical when the desired $\vartheta(r_1)$ has been defined.

Surface equations containing several constants have been developed, and it is now worthwhile to observe the physical significance of these constants.

The constant, C , is a constant of integration which simply moves the mirror along the z -axis. If the same value of C is used in both surface equations, the mirrors will automatically be spaced correctly to assure an afocal system providing constant optical path-length. The origin of the coordinate system may be positioned at will by a suitable choice of C . Sometimes in ray-tracing, it is desirable to move the origin of the coordinate system in order to center it on each mirror. In this case, each surface equation will use a different value of C , but then the mirror spacing must be accounted for separately.

The constant, b , is best defined in Equation (55). It may or may not correspond to a simple physical dimension. If, for instance,

the intensity transformation function is a constant, I , Equation (55) shows that

$$r_2^2 = \frac{r_1^2}{I} + b \quad .$$

Thus, when $r_1 = 0$, $r_2 = \sqrt{b}$. In this case, \sqrt{b} is the inside radius of the annular beam. This would also be true if $\vartheta(r_1) = r_1$, in which case

$$r_2^2 = 2r_1 + b \quad .$$

If, however, $\vartheta(r_1) = r_1^2$, Equation (55) yields

$$r_2^2 = 2\ln r_1 + b \quad .$$

In this case, when $r_1 \rightarrow 0$, corresponding to the axial ray, $r_2^2 \rightarrow -\infty$. This system clearly cannot be used with an input beam which contains the axial ray. Indeed, r_2 is imaginary whenever $\ln r_1^2 < -b$. With a suitable choice of b , this transformation could be used if both the input and output beams were annular.

Finally, if $\vartheta(r_1) = \exp(-r_1^2/2)$,

$$r_2^2 = 2e^{r_1^2/2} + b \quad .$$

Here, if $r_1 = 0$, $r_2 = \sqrt{2+b}$, again, the inside radius of the annular beam.

As has already been stated, k is the difference between the straight-line distance between the entrance and exit planes, and the OPL of a ray joining the planes through the optical system. This may be thought of as the excess OPL added by the system. However, this quantity becomes a system shape factor. Figure 8 presents the

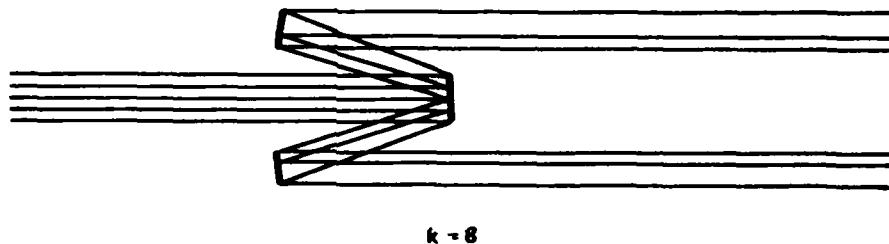
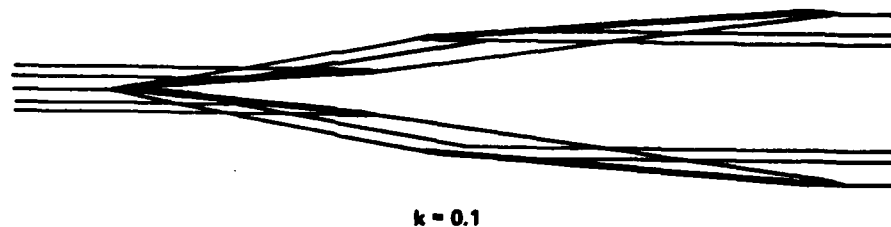


Figure 8. Grazing incidence (a) and normal-incidence (b) reflexicons ($I = 0.1$, $b = 1.5$).

meridional cross section of two systems. System (a) is a near-grazing-incidence system; System (b) is a near-normal-incidence system. It is clear from the drawing that the OPL between Planes A and B is very little more than the straight-line distance between them. Hence, k is small. In System (b), the OPL between A and B is much larger than the straight-line distance. In this case, k is large.

Thus, by varying k , the system can be varied from normal-incidence to grazing-incidence. The constant, k , permits varying the shape of the system to make it conform to the required physical dimensions, and

changing the angles of incidence on the mirror surfaces in order to take advantage of the improved reflectivity provided by the near-grazing-incidence systems. Also, a near-grazing-incidence design spreads the light beam over larger surface areas on the mirrors, thereby reducing the heat loading.

Now, having seen the types of design variation possible, we shall direct our attention to systems providing a specific intensity transformation.

1. Parabolic Reflaxicons

The surface equations have already been developed for a parabolic reflaxicon in which the geometrical axes of the parabolas are displaced from the optical axis of the system by a distance, a . The surfaces were found to be given by

$$z_1 = \frac{M-1}{2k} (r_1 + h)^2 + \frac{C}{k}$$

and

$$z_2 = \frac{M-1}{2kM} (r_2 + h)^2 + \frac{2C - k^2}{2k}$$

Now the intensity transformation which they provide will be examined.

Equation (39) shows that the ray-heights in the input and output beams are related by

$$\frac{r_2 + h}{r_1 + h} = M^* = \text{a constant}$$

Thus,

$$r_2 = (r_1 + h)M^* - h = M(r_1)r_1 \quad (58)$$

and

$$M(r_1) = \frac{(r_1 + h)M^* - h}{r_1} \quad (59)$$

Differentiating with respect to r_1 ,

$$\frac{dM(r_1)}{dr_1} = \frac{-(M^* - 1)h}{r_1^2}$$

But, by Equation (55),

$$[M(r_1)r_1]^2 = 2 \int \frac{r_1}{\vartheta(r_1)} dr_1 + b$$

Differentiating this expression with respect to r_1 ,

$$2[M(r_1)r_1] \left[M(r_1) + r_1 \frac{dM(r_1)}{dr_1} \right] = 2 \frac{r_1}{\vartheta(r_1)} \quad (60)$$

The intensity transformation function is, then,

$$\begin{aligned} \vartheta(r_1) &= \frac{r_1}{M(r_1)r_1 \left[M(r_1) + r_1 \frac{dM(r_1)}{dr_1} \right]} \\ &= \frac{r_1}{[(r_1 + h)M^* - h] \left[\frac{(r_1 + h)M^* - h - (M^* - 1)h}{r_1} \right]} \\ &= \frac{r_1}{(r_1 + h)M^{*2} - M^*h} \end{aligned} \quad (61)$$

A specific case will now be examined. Let the input beam have a radius of 1, and an intensity of $I_1 = 1$. Let $h = 1$, and $M^* = 3$. This will give an annular output beam having an inside radius of 2, and an outside radius of 5. Figure 9 shows the radial intensity distribution across the annular beam. For comparison, an equivalent

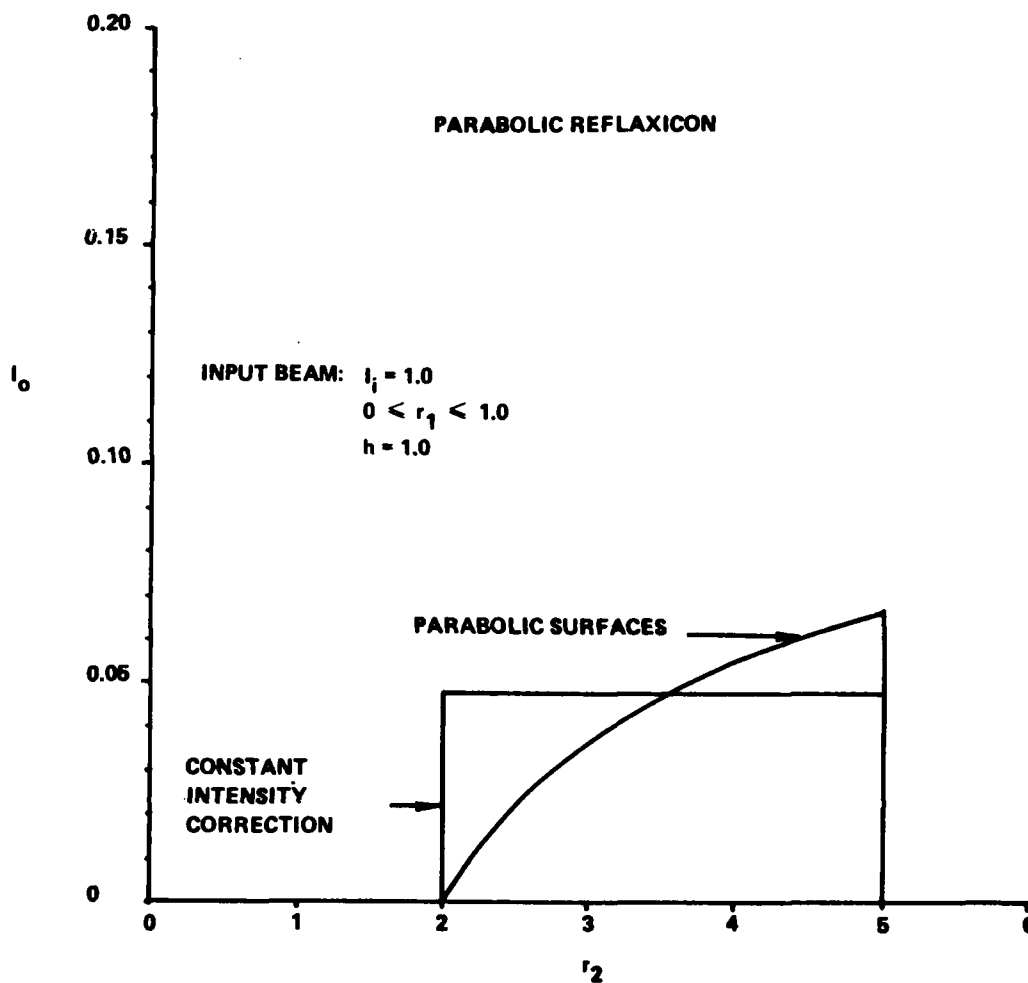


Figure 9. Radial energy distribution of parabolic reflaxicon, compared with equivalent constant intensity distribution.

annular beam of uniform intensity is shown. In this case, the intensity transformation function for the beam of constant intensity is $\phi(r_1) = 1/21$.

2. Constant Intensity Reflaxicons

The constant intensity transformation is especially useful in high-energy laser systems. The input and output beams will have

the same radial energy distribution, i.e., a uniform cylindrical input beam will be transformed into a uniform annular beam; a Gaussian cylindrical beam will be transformed into a Gaussian annular beam, et cetera. Of course, the reverse transformations are just as easily accomplished.

If, in the surface Equations (56) and (57), $\phi(r_1)$ is a constant, I , we have for the first mirror:

$$\begin{aligned} z_1 &= \frac{\int \left(\frac{2}{I} r_1 dr_1 + b \right)^{\frac{1}{2}} dr_1 - \frac{1}{2} r_1^2 + C}{k} \\ &= \frac{\int \left(\frac{r_1^2}{I} + b \right)^{\frac{1}{2}} dr_1 - \frac{1}{2} r_1^2 + C}{k} \end{aligned} \quad (62)$$

or,

$$z_1 = \frac{\frac{1}{2\sqrt{I}} \left\{ r_1 \left(r_1^2 + Ib \right)^{\frac{1}{2}} + Ib \ln \left[r_1 + \left(r_1^2 + Ib \right)^{\frac{1}{2}} \right] \right\} - \frac{1}{2} r_1^2 + C}{k} \quad (63)$$

Similarly, for the second mirror, we find that

$$\begin{aligned} z_2 &= \frac{\frac{1}{I} \int r_1 dr_1 + \frac{b}{2} - r_1 \left(\frac{2}{I} \int r_1 dr_1 + b \right)^{\frac{1}{2}}}{k} \\ &+ \frac{\int \left(\frac{2}{I} \int r_1 dr_1 + b \right)^{\frac{1}{2}} dr_1 - \frac{k^2}{2} + C}{k} \end{aligned} \quad (64)$$

$$\begin{aligned}
z_2 &= \frac{\frac{r_1^2}{2I} + \frac{b}{2} - r_1 \left(\frac{r_1^2}{I} + b \right)^{\frac{1}{2}} + \int \left(\frac{r_1^2}{I} + b \right)^{\frac{1}{2}} dr_1 - \frac{k^2}{2} + C}{k} \\
&= \frac{\frac{r_1^2}{2I} + \frac{b}{2} - \frac{r_1}{\sqrt{I}} \left(r_1^2 + Ib \right)^{\frac{1}{2}}}{k} \\
&\quad + \frac{\frac{1}{2\sqrt{I}} \left\{ r_1 \left(r_1^2 + Ib \right)^{\frac{1}{2}} + Ib \ln \left[r_1 + \left(r_1^2 + Ib \right)^{\frac{1}{2}} \right] \right\}}{k} - \frac{k^2}{2} + C \\
&= \frac{\frac{r_1^2}{2I} + \frac{b}{2} - \frac{1}{2\sqrt{I}} \left\{ r_1 \left(r_1^2 + Ib \right)^{\frac{1}{2}} \right.}{k} \\
&\quad \left. + \frac{-Ib \ln \left[r_1 + \left(r_1^2 + Ib \right)^{\frac{1}{2}} \right] \right\} - \frac{k^2}{2} + C}{k}
\end{aligned}$$

and

$$r_2 = \left[2 \int \frac{r_1}{I} dr_1 + b \right]^{\frac{1}{2}} = \frac{1}{\sqrt{I}} \left[r_1^2 + Ib \right]^{\frac{1}{2}}$$

Writing Equation (60) in terms of r_2 ,

$$z_2 = \frac{r_2^2 - r_2 \left[(r_2^2 - b)I \right]^{\frac{1}{2}} + b\sqrt{I} \ln \left\{ \left[(r_2^2 - b)I \right]^{\frac{1}{2}} + r_2\sqrt{I} \right\} - k^2 + 2C}{k}$$

(65)

Figures 10, 11, and 12, illustrate some of the possible forms of the constant-intensity reflaxicon. The reflaxicons in Figures 10 and 11 accomplish exactly the same thing; only the shape factor, k , has been varied. Careful inspection of these two figures will show a very peculiar feature of the mirrors. They have both positive and negative regions. The inner mirror is concave near the point and convex near the rim. The outer mirror has, of course, exactly the same slopes, but the convex region, corresponding to the concave

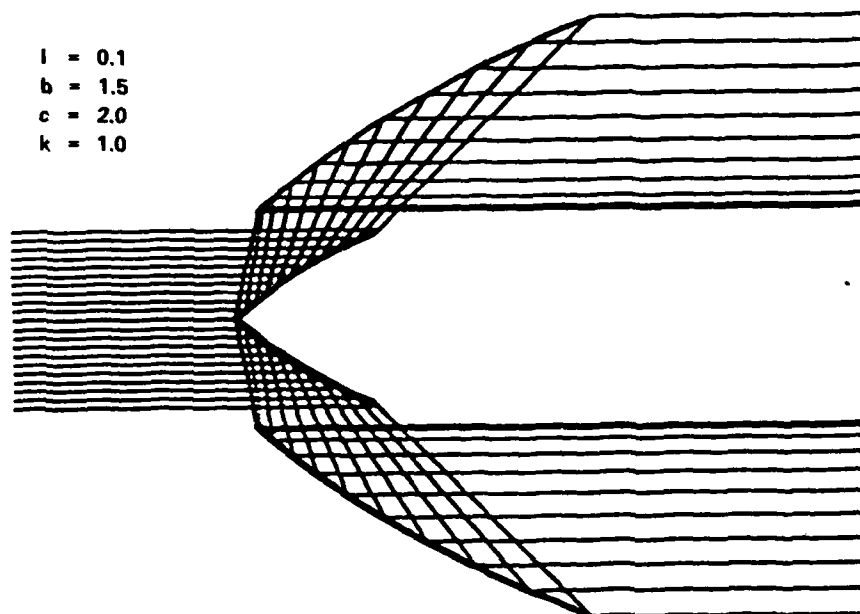


Figure 10. Forward-reflecting constant-intensity reflexicon.

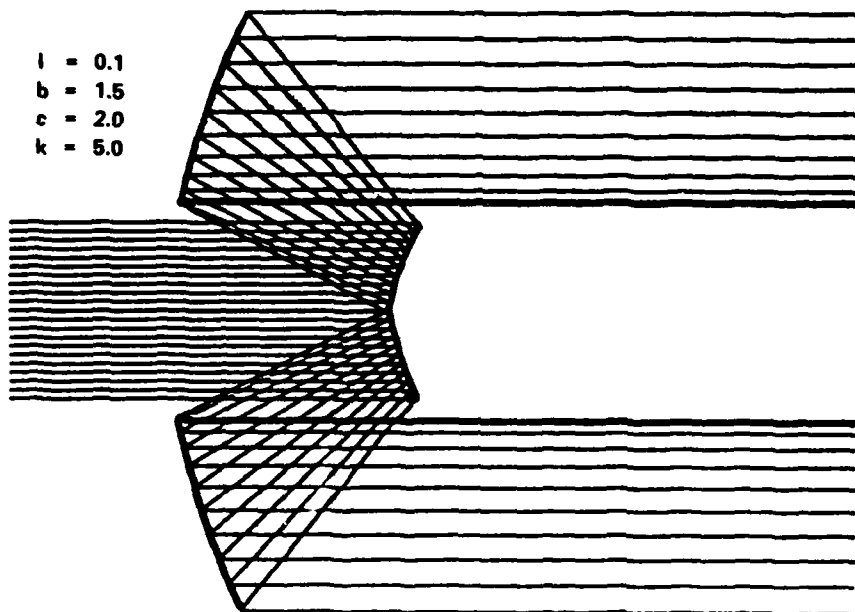


Figure 11. Near-normal-incidence constant-intensity reflexicon.

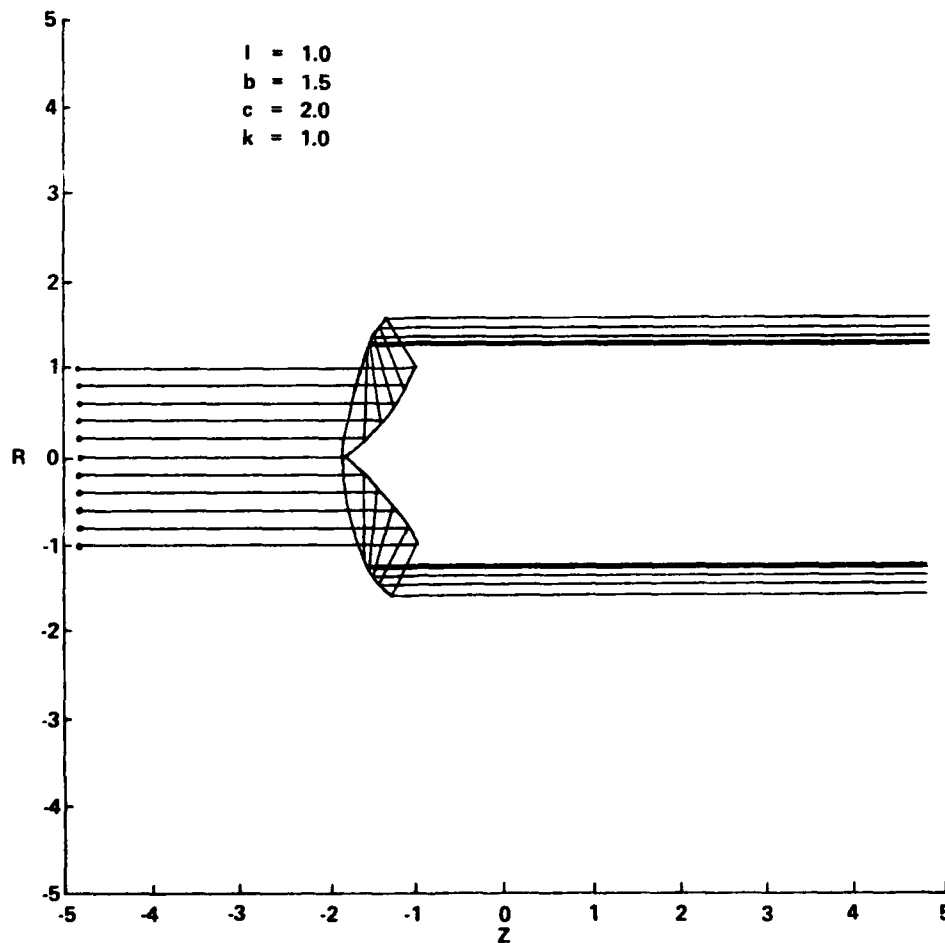


Figure 12. Constant-intensity reflaxicon giving unit beam-intensity transformation.

region of the inner mirror, is confined to a very narrow zone about the inner edge of the mirror.

The packing of the rays near the inner boundary of the annular beam does not indicate that the beam is brighter at the inside boundary than it is at the outside. This ray-packing only compensates for fall-off in intensity at the inside boundary, which exists in an uncompensated system.

The system in Figure 12, giving a unit intensity transformation, does not show an inflection zone, but the same S-shaped curve would be present if the mirror surface were extended far enough. Thus, these surfaces are properly termed "ogees-of-revolution."

Clearly, the surfaces used in these systems are virtually impossible to manufacture by classical optical grinding and polishing techniques. They are, however, well within the capabilities of single-point diamond turning.

The ray-trace analysis will show that these ogees-of-revolution are extremely sensitive to alignment errors, and every reasonable effort must be made to assure high-precision alignment.

Chapter III. WAXICON SYSTEMS

A. Generalized Surface Equations

Generalized surface equations for the waxicon will now be developed analogous to those developed for the reflaxicon. The same two conditions will be imposed that were imposed on the reflaxicon system, i.e., constant path-length and afocality. There is one significant difference. In the reflaxicon, the slopes of the two mirrors at the ray-intercepts were required to be equal; the waxicon requires the tangents to the surfaces to be at right angles to one another. This makes the system retroreflecting as well as afocal. Also, the entrance and exit planes may now be represented by a single plane with the rays passing through it from both directions.

In Figure 13, a ray propagating from the reference plane, $z = z_0$, through the system and back to the reference plane will travel a total distance given by

$$\text{OPL} = z_1 - z_0 + \sqrt{(z_2 - z_1)^2 + (r_2 - r_1)^2} + z_2 - z_0 = L \quad (66)$$

= a constant.

Then,

$$\sqrt{(z_2 - z_1)^2 + (r_2 - r_1)^2} = L + 2z_0 - z_1 + z_2 = H - (z_1 + z_2) \quad (67)$$

where H is a constant. The mathematics which follows can be simplified by translating the coordinate system along the z -axis by an amount $H/2$,

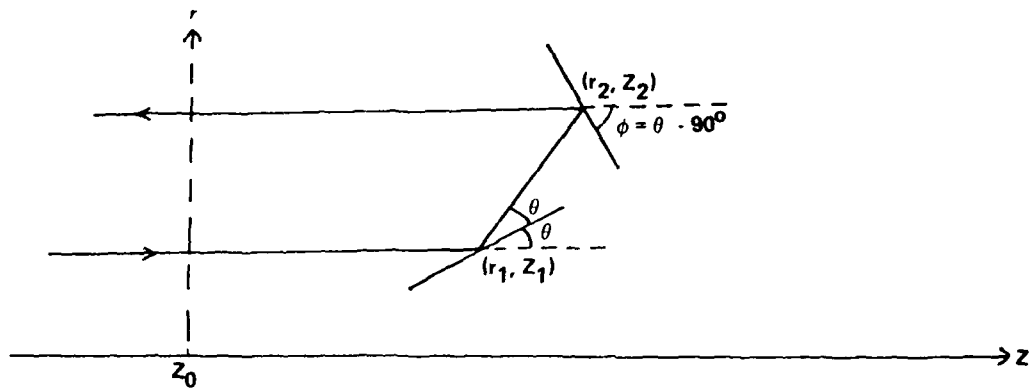


Figure 13. Diagram of waxicon system.

so z_1 and z_2 become $z_1 + H/2$ and $z_2 + H/2$, respectively. Equation (67) then becomes

$$\sqrt{(z_2 - z_1)^2 + (r_2 - r_1)^2} = H - (z_1 + z_2) - H = -(z_1 + z_2) \quad (68)$$

This involves no loss of generality. Squaring both sides of the equation, we find that:

$$(z_2 - z_1)^2 + (r_2 - r_1)^2 = (z_1 + z_2)^2 \quad (69)$$

or,

$$(r_2 - r_1)^2 = 4 z_1 z_2 \quad (70)$$

This is the condition for constant path-length.

From the preceding figure, it can be seen that

$$\tan 2\theta = \frac{r_2 - r_1}{z_2 - z_1} \quad (71)$$

and

$$\tan \theta = \frac{dr_1}{dz_1} = - \frac{dz_2}{dr_2} \quad (72)$$

$$\tan \theta = \frac{-1 \pm \sqrt{1 - \tan^2 2\theta}}{\tan 2\theta} = \frac{-1 \pm \sqrt{\frac{(z_2 - z_1)^2 - (r_2 - r_1)^2}{(z_2 - z_1)^2}}}{\frac{r_2 - r_1}{z_2 - z_1}}$$

$$= \frac{-(z_2 - z_1) \pm \sqrt{(z_2 - z_1)^2 - (r_2 - r_1)^2}}{r_2 - r_1}$$

Substituting $4z_1z_2$ for $(r_2 - r_1)^2$, the preceding equation becomes

$$\tan \theta = \frac{-(z_2 - z_1) \pm (z_1 + z_2)}{r_2 - r_1} \quad (73)$$

Taking the positive sign will yield imaginary or complex solutions.

Therefore, the negative sign will be used. Then,

$$\tan \theta = \frac{-2z_2}{r_2 - r_1} = \frac{-2z_2}{[M(r_1) - 1]r_1} = \frac{dr_1}{dz_1} = -\frac{dz_2}{dr_2} \quad (74)$$

The equation for the outer mirror is, then,

$$\int \frac{dz_2}{2z_2} = \int \frac{dr_2}{r_2 - r_1} \quad (75)$$

or,

$$\ln z_2 = 2 \int \frac{dr_2}{r_2 - r_1} + \ln C \quad (76)$$

where $\ln C$ is the constant of integration.

The equation for the inner mirror can be written very simply as a function of the outer mirror by combining the constant path-length and slope equations.

From Equation (74), we see that:

$$\left(\frac{dr_1}{dz_1}\right)^2 = \frac{4z_2^2}{(r_2 - r_1)^2} \quad (77)$$

But the condition for constant path-length requires that

$$(r_2 - r_1)^2 = 4 z_1 z_2 .$$

Then,

$$\frac{4 z_2^2}{(r_2 - r_1)^2} = \frac{4 z_2^2}{4 z_1 z_2} , \quad (78)$$

or,

$$\frac{4 z_2^2}{(r_2 - r_1)^2} = \frac{z_2}{z_1} . \quad (79)$$

Solving this equation for z_1 , the following is obtained:

$$z_1 = \frac{(r_2 - r_1)^2 z_2}{4 z_2^2} = \frac{(r_2 - r_1)^2}{4 z_2} . \quad (80)$$

We shall now direct our attention to the intensity transformation in waxicons.

B. Intensity Transformation

The waxicon gives a radial inversion of the input beam. The inside rim-rays of the input beam are transformed into the outside rim-rays of the output beam, and conversely. If an input annulus has an inside radius of r_1 and an outside radius of $r_1 + \xi$, the output beam of the waxicon will have an inside radius of $(r_1 + \xi)M(r_1 + \xi)$, and an outside radius of $r_1 M(r_1)$. The reflaxicon, on the other hand, would have an output beam with an inside radius of $r_1 M(r_1)$, and an outside radius of $(r_1 + \xi)M(r_1 + \xi)$. In either case, the area of the input annulus would be

$$A_1 = \pi [(r_1 + \xi)^2 - r_1^2] . \quad (81)$$

The output annulus of the waxicon would have an area of

$$A_{2_w} = \pi \left\{ [r_1 M(r_1)]^2 - [(r_1 + \xi) M(r_1 + \xi)]^2 \right\}, \quad (82)$$

and that of the reflaxicon, an area of

$$A_{2_r} = \pi \left\{ [(r_1 + \xi) M(r_1 + \xi)]^2 - [r_1 M(r_1)]^2 \right\}. \quad (83)$$

Combining Equations (46), (81), and (83), in the case of the reflaxicon, it can be seen that

$$\begin{aligned} \vartheta(r_1) &= \frac{(r_1 + \xi)^2 - r_1^2}{[(r_1 + \xi) M(r_1 + \xi)]^2 - [r_1 M(r_1)]^2} \\ &= \frac{1}{[M(r_1)]^2 + r_1 M(r_1) \frac{dM(r_1)}{dr_1}}. \end{aligned} \quad (84)$$

In the case of the waxicon, combining Equations (46), (81), and (82), yields

$$\begin{aligned} \vartheta(r_1) &= \frac{(r_1 + \xi)^2 - r_1^2}{[r_1 M(r_1)]^2 - [(r_1 + \xi) M(r_1 + \xi)]^2} \\ &= - \frac{(r_1 + \xi)^2 - r_1^2}{[(r_1 + \xi) M(r_1 + \xi)]^2 - [r_1 M(r_1)]^2} \\ &= \frac{-1}{[M(r_1)]^2 + r_1 M(r_1) \frac{dM(r_1)}{dr_1}}. \end{aligned} \quad (85)$$

The negative sign does not imply a negative intensity, but only a reverse ordering of the rays. We now have the following differential equation:

$$\frac{dM(r_1)}{dr_1} r_1 M(r_1) + [M(r_1)]^2 + \frac{1}{\vartheta(r_1)} = 0. \quad (86)$$

It will be noted that this is exactly the differential equation obtained for the reflaxicon, except that $\vartheta(r_1)$ has been replaced by $-\vartheta(r_1)$. Hence, the solution is

$$[M(r_1)r_1']^2 = -2 \int \frac{r_1 dr_1}{\vartheta(r_1)} + b = r_2^2 \quad (87)$$

Substitution of this expression into the waxicon surface equations provides a general solution for all $\vartheta(r_1)$.

The surface equation for the outer mirror becomes

$$\ln z_2 = 2 \int \frac{dr_z}{\left[b - 2 \int \frac{r_1 dr_1}{\vartheta(r_1)} \right]^{\frac{1}{2}} - r_1} + \ln C \quad (88)$$

and that of the inner mirror becomes

$$z_1 = \frac{\left\{ \left[b - 2 \int \frac{r_1 dr_1}{\vartheta(r_1)} \right]^{\frac{1}{2}} - r_1 \right\}^2}{4 z_2} \quad (89)$$

The surface equation for the outer mirror can easily be written as a function of r_1 and $\vartheta(r_1)$ alone by differentiating Equation (87) with respect to r_1 to obtain the expression

$$dr_2 = \frac{r_1 dr_1}{\vartheta(r_1)r_2} \quad (90)$$

or,

$$dr_2 = \frac{r_1}{\vartheta(r_1) \left[b - 2 \int \frac{r_1 dr_1}{\vartheta(r_1)} \right]^{\frac{1}{2}}} dr_1 \quad (91)$$

Equation (88) then becomes

$$\ln z_2 = 2 \int \frac{r_1 dr_1}{g(r_1) \left[b - 2 \int \frac{r_1 dr_1}{(r_1)} \right]^{\frac{1}{2}} \left\{ \left[b - 2 \int \frac{r_1 dr_1}{(r_1)} \right]^{\frac{1}{2}} - r_1 \right\}} + \ln C .$$

C. Constant Intensity Wavicons

If the intensity transformation function assumes the constant value, I , it can be seen that Equation (87) becomes

$$r_2^2 = b - 2 \int \frac{r_1 dr_1}{I} = b - \frac{r_1^2}{I} , \quad (93)$$

and

$$r_1^2 = (b - r_2^2) I . \quad (94)$$

Thus, the surface equation for the outer mirror is

$$\ln z_2 = 2 \int \frac{dr_2}{r_2 - \sqrt{I(b - r_2^2)}} . \quad (95)$$

In order to integrate this expression, the following change of variables is made:

$$r_2 = \sqrt{b} \cos \phi$$

$$dr_2 = -\sqrt{b} \sin \phi d\phi$$

$$\phi = \arccos \frac{r_2}{\sqrt{b}} = \arctan \frac{\sqrt{b - r_2^2}}{r_2} . \quad (96)$$

Then,

$$\sqrt{I(b - r_2^2)} = \sqrt{Ib - Ib \cos^2 \phi} = \sqrt{Ib \sin^2 \phi} \quad (97)$$

and

$$\ln z_2 = 2 \int \frac{-\sqrt{b} \sin \phi d\phi}{\sqrt{b} \cos \phi - \sqrt{Ib} \sin \phi} + \ln C = -2 \int \frac{\tan \phi d\phi}{1 - \sqrt{I} \tan \phi} + \ln C . \quad (98)$$

Integrating, we have,

$$\begin{aligned}\ln z_2 &= \frac{2}{I+1} \left[\sqrt{I} \phi + \ln (\cos \phi - \sqrt{I} \sin \phi) \right] + \ln C \\ &= \frac{2}{I+1} \left[\sqrt{I} \arctan \frac{\sqrt{b-r_2^2}}{r_2} + \ln \left(\frac{r_2}{\sqrt{b}} - \sqrt{I} \sqrt{\frac{b-r_2^2}{b}} \right) \right] + \ln C \quad (99)\end{aligned}$$

Since $(-1/I+1)\ln b + \ln C$ is a constant, these terms may be written as a single constant, $\ln C$. This new constant becomes a system shape factor, in the same manner as k in the reflexicon system. Equation (99) may now be written

$$\ln z_2 = \frac{2}{I+1} \left[\sqrt{I} \arctan \frac{\sqrt{b-r_2^2}}{r_2} + \ln \left(r_2 - \sqrt{I(b-r_2^2)} \right) \right] + \ln C \quad (100)$$

Taking the exponential of both sides,

$$z_2 = C \left[r_2 - \sqrt{I(b-r_2^2)} \right]^{\frac{2}{I+1}} \exp \left[\frac{2\sqrt{I}}{I+1} \arctan \frac{\sqrt{b-r_2^2}}{r_2} \right] \quad (101)$$

The surface equation for the inner mirror is now

$$z_1 = \left[\left(b - \frac{r_1^2}{I} \right)^{\frac{1}{2}} - r_1 \right]^2$$

or

$$z_1 = \frac{\left[\left(b - \frac{r_1^2}{I} \right)^{\frac{1}{2}} - r_1 \right]^2}{4C \left[r_2 - \sqrt{I(b-r_2^2)} \right]^{\frac{2}{I+1}} \exp \left[\frac{2\sqrt{I}}{I+1} \arctan \frac{\sqrt{b-r_2^2}}{r_2} \right]}$$

or

$$z_1 = \frac{\left[\left(b - \frac{r_1}{I} \right)^{\frac{1}{2}} - r_1 \right]^2}{4C \left[\left(b - \frac{r_1^2}{I} \right)^{\frac{1}{2}} - r_1 \right]^{\frac{2}{I+1}} \exp \left[\frac{2\sqrt{I}}{I+1} \arctan \frac{r_1}{\left(b - \frac{r_1^2}{I} \right)^{\frac{1}{2}}} \right]} \quad (102)$$

Turning now to the meaning of the constants in the waxicon surface equations, Equation (94) shows that when $r_1 = 0$, corresponding to the axial ray, $r_2 = \sqrt{b}$. Since the axial input-ray is reflected into the outside rim of the annular beam, \sqrt{b} is the radius of the outside rim. Compare this to the case of the constant-intensity reflaxicon, in which \sqrt{b} was the radius of the inside rim of the annular beam. This points out, again, the radial inversion of the beam in the waxicon.

As has been mentioned, the constant, C , functions as a system shape-factor. When C is very small, the inner mirror will be used at near grazing-incidence, and the outer mirror will work at near normal-incidence. The reverse is true when C is large. Figures 14, 15, and 16 illustrate this variation with C .

Waxicons are usually made in a configuration similar to that in Figure 15. As has been pointed out by David Fink¹, if waxicons are

¹David Fink, "Polarization Effects of Axicons," Applied Optics, Vol. 18, March 1979, p. 581.

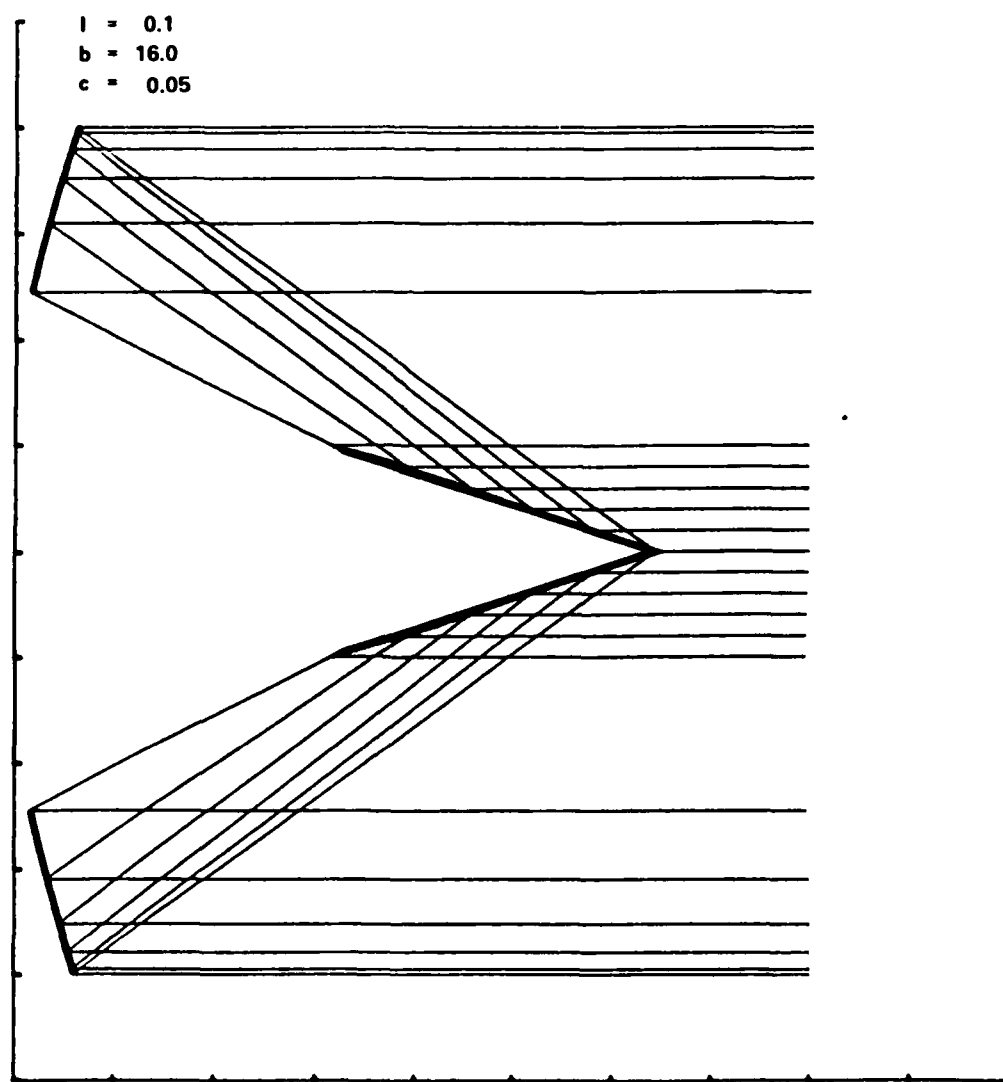


Figure 14. Waxicon with near-grazing-incidence on the inner mirror.

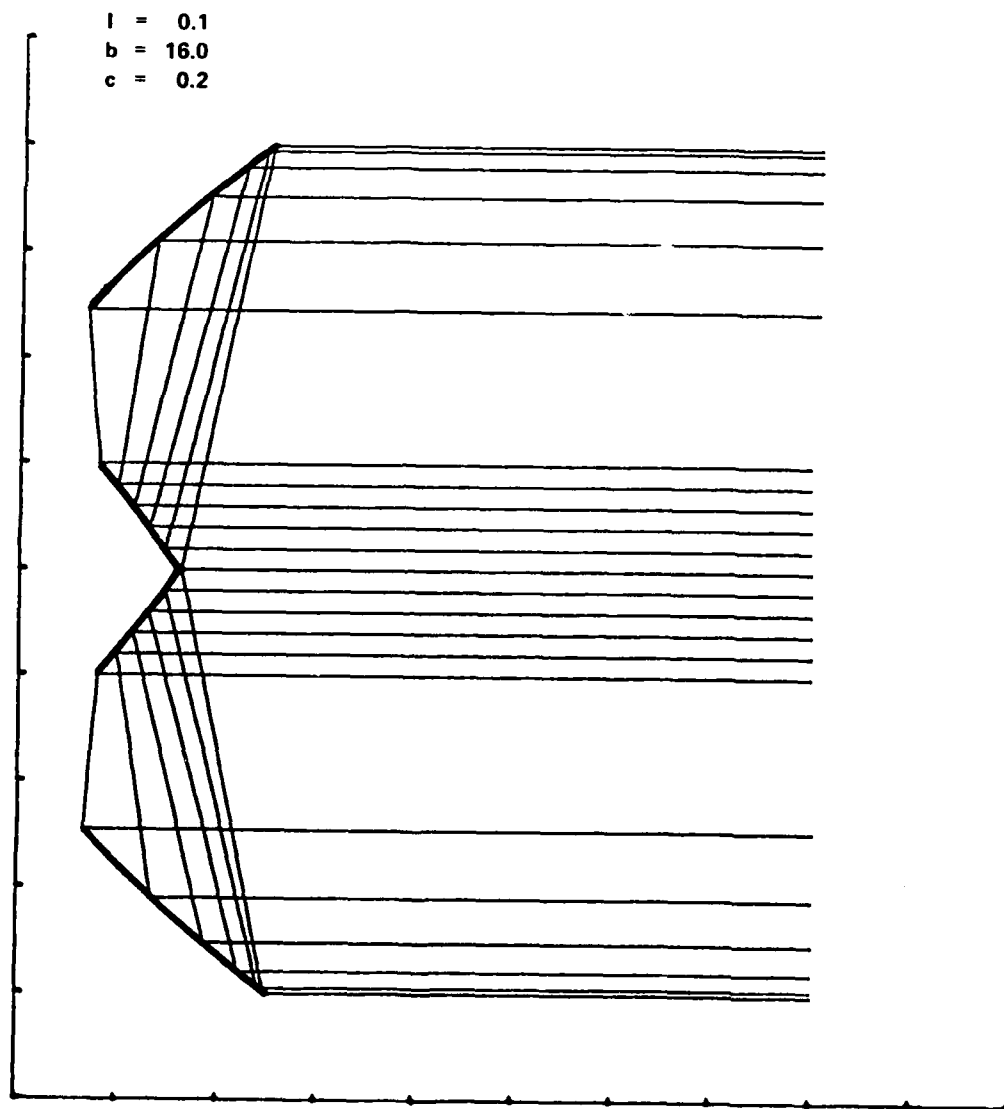


Figure 15. Waxicon with nearly equal angles of incidence on both mirrors.

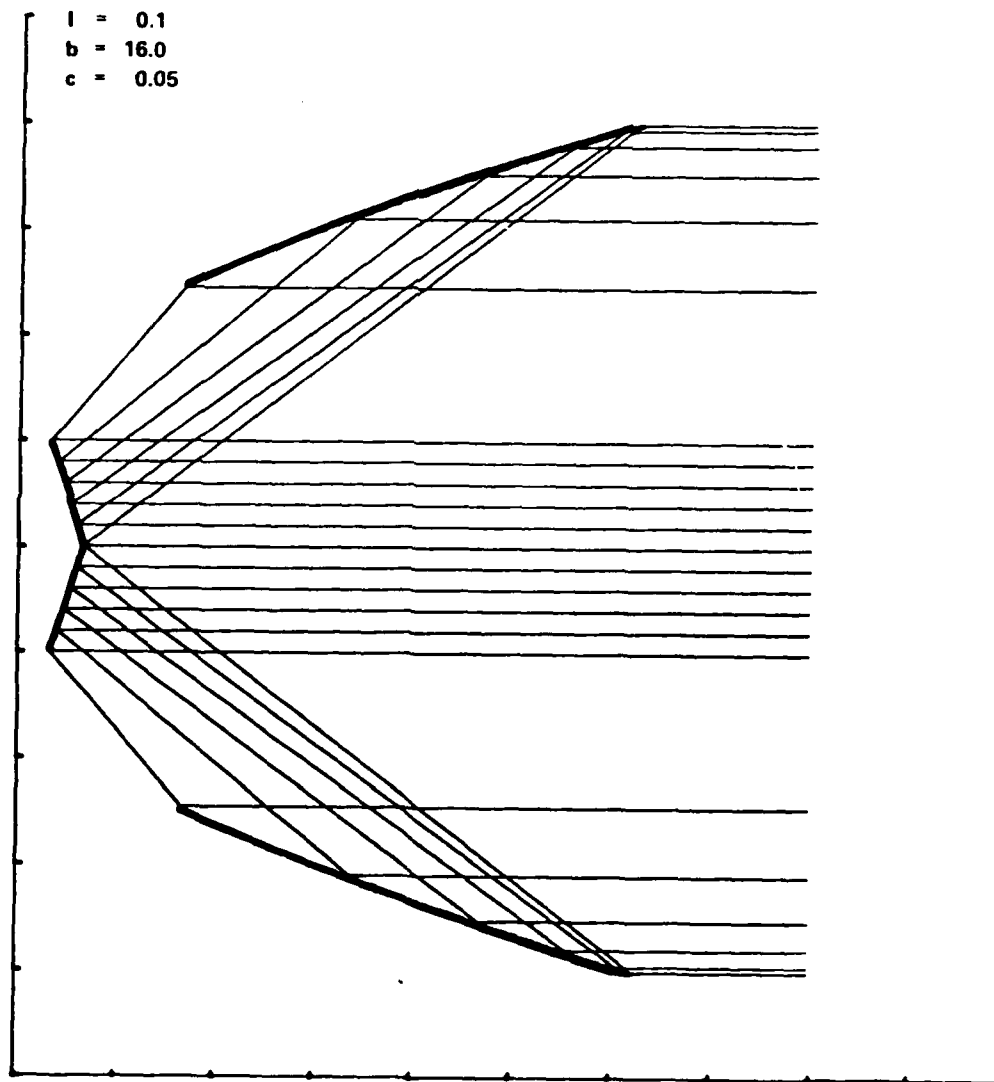


Figure 16. Waxicon with near-grazing-incidence
on the outer mirror.

dielectric coated, the polarization direction of the output beam is rotated through an angle of 2θ , where θ is the azimuthal angle around the annulus. This can cause beam cancellation, clearly an undesirable consequence. This can be prevented, however, by making one reflection at less than Brewster's angle, and the other greater. A waxicon, such as that in Figure 15, in which the angles of reflection at the two mirrors are roughly equal, would almost always give polarization problems. However, the polarization problem can be alleviated by using designs similar to those in Figures 14 and 16, in which one angle is large and the other small. With metallic coatings, waxicaons similar to the one in Figure 15 provide a more compact system.

It is interesting to note that reflaxicons do not present this polarization problem.

Chapter IV. PERFORMANCE ANALYSIS

A. Ray-Tracing Procedures

Attention is now directed to the practical design of reflexicons and waxicons. One of the most serious problems in the use of these systems is the sensitivity to alignment error. This can be readily anticipated, because of the complexity of the surfaces. This sensitivity was investigated by means of exact ray-tracing. Third- and fifth-order theory is of little value in analyzing the performance of these systems in the configurations in which they are usually made, because small-angle approximations are inadequate for the angles involved.

An extremely versatile ray-trace computer program has been developed by Dietrich Korsch². This program ray-traces systems of conic sections of revolution, using exact formulas, and allows the tilt of each component about two axes orthogonal to the optical axis, and displacements along all three axes. It provides data-options of centroid shift, root mean square (rms) spot-size about the centroid in both the Gaussian and best-focus planes, intensity distribution within the image of a point-source, field curvature, and spot-diagrams. The program has been modified to give angular, as well as linear measurements, rms decollimation, and a statistical output-beam

²Dietrich Korsch, "Ray Trace Evaluation Program," Vol. 1, Teledyne Brown Engineering, Huntsville, Alabama, 1977.

evaluation when all misalignment parameters are chosen randomly within specified limits. The program was expanded to accept the complicated surface equations, characteristic of reflaxicons and waxicons.

The intersections of the rays with the surfaces were found by iteration in all misaligned cases. At first, the Newton-Raphson iteration scheme was used, but it was found that the iteration frequently did not converge. The iteration was then changed to the regula falsi, or false position scheme, which was made to work reliably.

B. Reflaxicon Systems

As a basis for our analysis, a reflaxicon of a configuration will be chosen that would be suitable for use in high-energy laser systems as a beam-shaper or as a beam expander. The system will be required to give a constant intensity transformation, and the cylindrical beam will have an intensity ten times that of the annular beam, i.e., $I = 0.1$. The cylindrical beam will have a radius of $\sqrt{1.5}$, being just large enough to allow adequate space for mounting the inside mirror, without its interfering with the annular beam. This would allow its use in conjunction with conventional optical systems of moderate size, and would minimize the cost of the reflaxicon beam shaper.

The shape factor, k , will be given a value of unity, making the mirrors forward reflecting. This system is very different from normal-incidence and grazing-incidence systems. The angles of incidence are large, and no small-angle approximations are valid. The constant, C , may be arbitrarily chosen, unless otherwise noted.

For the actual ray-tracing, the origin is shifted for each mirror in order that tilt variations will not be made about a distant origin. If the origin is far removed from the mirror, a tilt of the mirror about that origin would result in a large lateral displacement of the mirror. This would make it impossible to study the effects of tilt without significant decentering of the mirror. For each surface, the origin was arbitrarily shifted to such a position on the z-axis, that the intercept of a ray having an initial height of $r_1 = 0.5$ in the cylindrical beam would fall over the origin, except in the case where the origin was being deliberately shifted in order to determine the effect of tilting the mirrors about various pivot-points.

The misalignment errors in the afocal reflaxicon fall into three types. They are angular misalignment of one mirror with respect to the other, a decentering of one mirror relative to the other, and a tilt of the whole system with respect to the input beam.

Since the input beam is collimated, a lateral, or longitudinal shift of the whole system has no effect on the collimation of the annular beam. It would change the intensity profile of the annular beam, however, unless the input beam were of uniform intensity.

In the afocal reflaxicon system, either a decentering or a tilt of the inner mirror can be thought of as a decentering or a tilting of the outer mirror with a corresponding misalignment of the whole system with respect to the input beam. Therefore, only tilt, decenter, and despace on the outer mirror will be considered as well as an off-axis tilt of the whole system with respect to the input beam.

1. Mirror Tilt

The effect of the shape factor, k , on the sensitivity to a tilt error can be seen by choosing a fixed tilt angle of 0.1 mrad for the outer mirror, and computing the rms decollimation of the output beam for several values of k . This tilt angle may seem large, but it must be remembered that a system which would possibly require alignment in the field with minimal alignment equipment is being examined. The relationship between the rms decollimation produced by this tilt, and the shape factor, is seen in Figure 17.

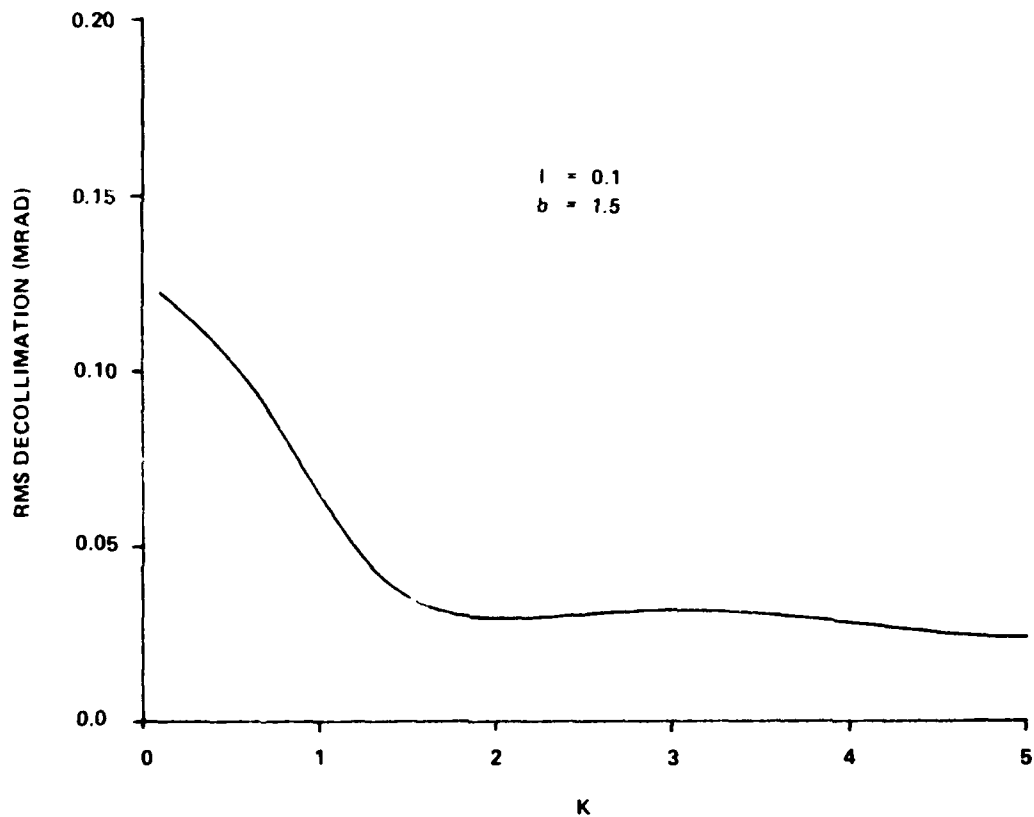


Figure 17. Beam decollimation produced by a constant tilt of 0.1 mrad on the outer mirror, as a function of shape factor.

It is noted that the grazing-incidence systems, represented by a small k , are considerably more sensitive to tilt than the normal-incidence systems, in which k would be larger than approximately four.

The direction of the annular beam will be changed by this tilt of the outer mirror, and its dependence on k can be seen in Figure 18. Clearly, the centroid shift increases sharply with increasing k , although with the 0.1-mrad tilt, the centroid shift is still quite small. Figure 18 illustrates conspicuously the effect of the location of the origin when tilt is present. Notice that the centroid shift is negative in the $k = 0$ to $k = 1$ region. This shift is in the opposite direction to the mirror tilt. As seen in Figure 10, the outer mirror is a very deep, barrel-shaped mirror, and the origin was placed near its center. As will be seen, the system is very sensitive to decentering. The inside region of the mirror, which contains the most complicated part of the surface, is decentered in the opposite direction of the mirror tilt. This introduces a negative component in the centroid shift. Since this region of the mirror contains a convex rim and an inflection of the curve, it is more sensitive to the negative decentering than the remainder of the mirror is to its positive decentering. The tilt contributes an extremely small positive centroid shift, and is overpowered by the negative decentering. If the origin were placed behind the inside edge of the outer mirror, the resultant decentering would be positive, and there would be a relatively large positive centroid shift.

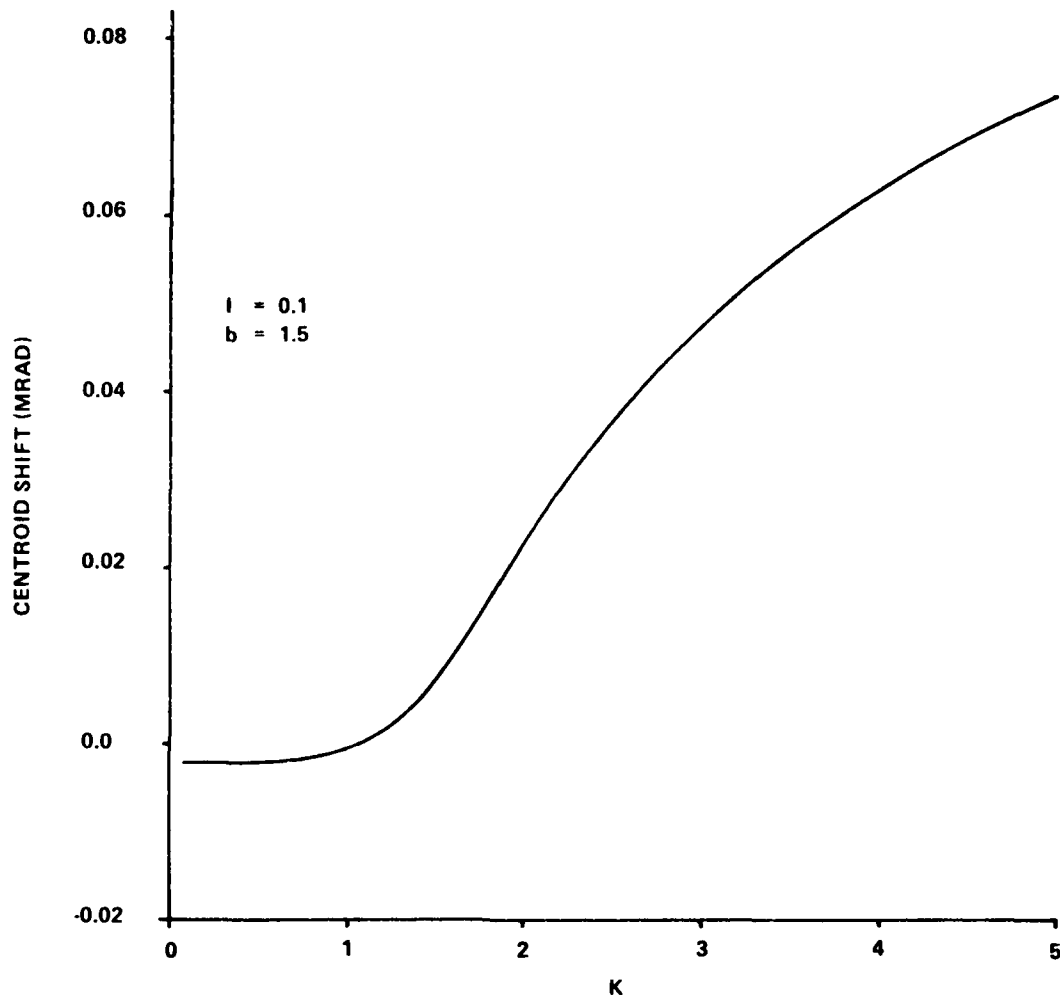


Figure 18. Centroid shift produced by constant tilt of 0.1 mrad on the outer mirror, as a function of the shape factor.

If the shape factor, k , is held constant, and the tilt angle is varied, then the rms decollimation varies linearly with tilt angle (Figure 19). Also, the effect is shown in Figure 17, since each k produces a different slope. This linear variation of decollimation with tilt is indicative of coma.

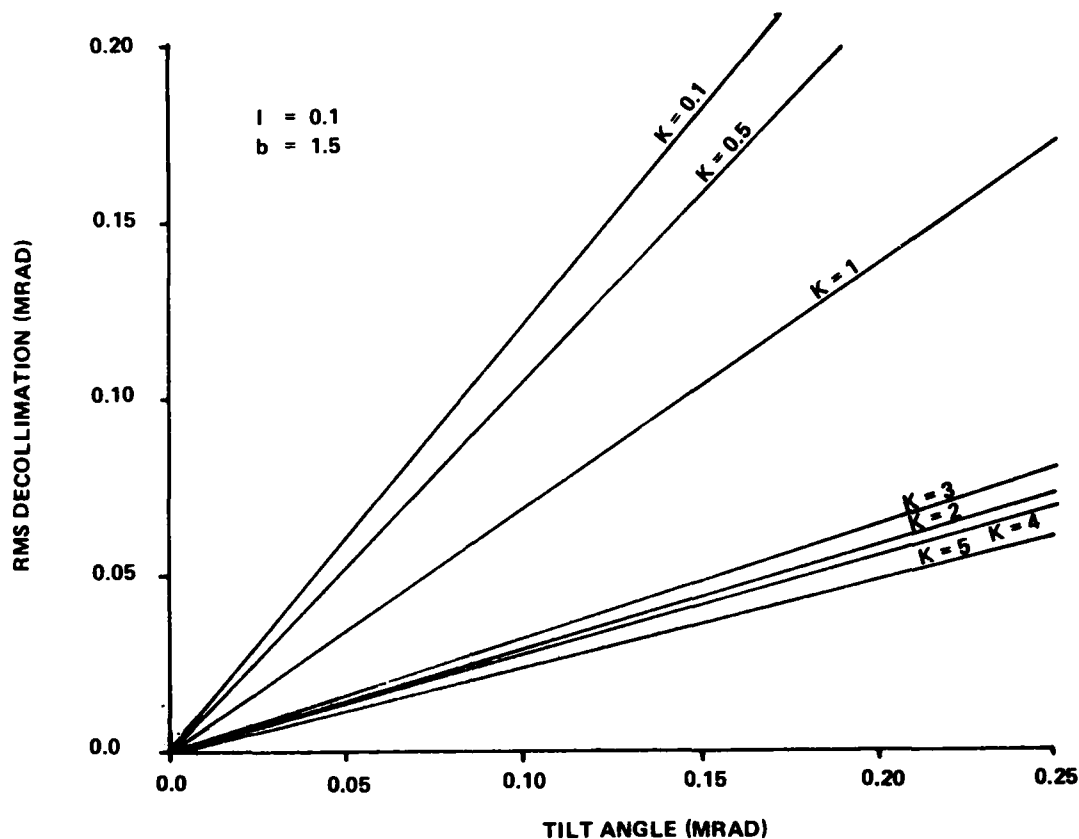


Figure 19. Beam decollimation versus tilt of outer mirror.

The beam decollimation is also dependent on the location of the axial point about which the tilt occurs. Figure 20 shows this dependence. The decollimation is minimized when the pivot-point lies almost exactly in the plane of the inside edge of the outer mirror. It is at this edge that the mirror has the strongest curvature, and the most rapid change in curvature. Whenever possible, reflexicons should be designed with the mounting surface of the outer mirror so positioned that any tilt will occur about a point as close to the plane of the inside edge as possible.

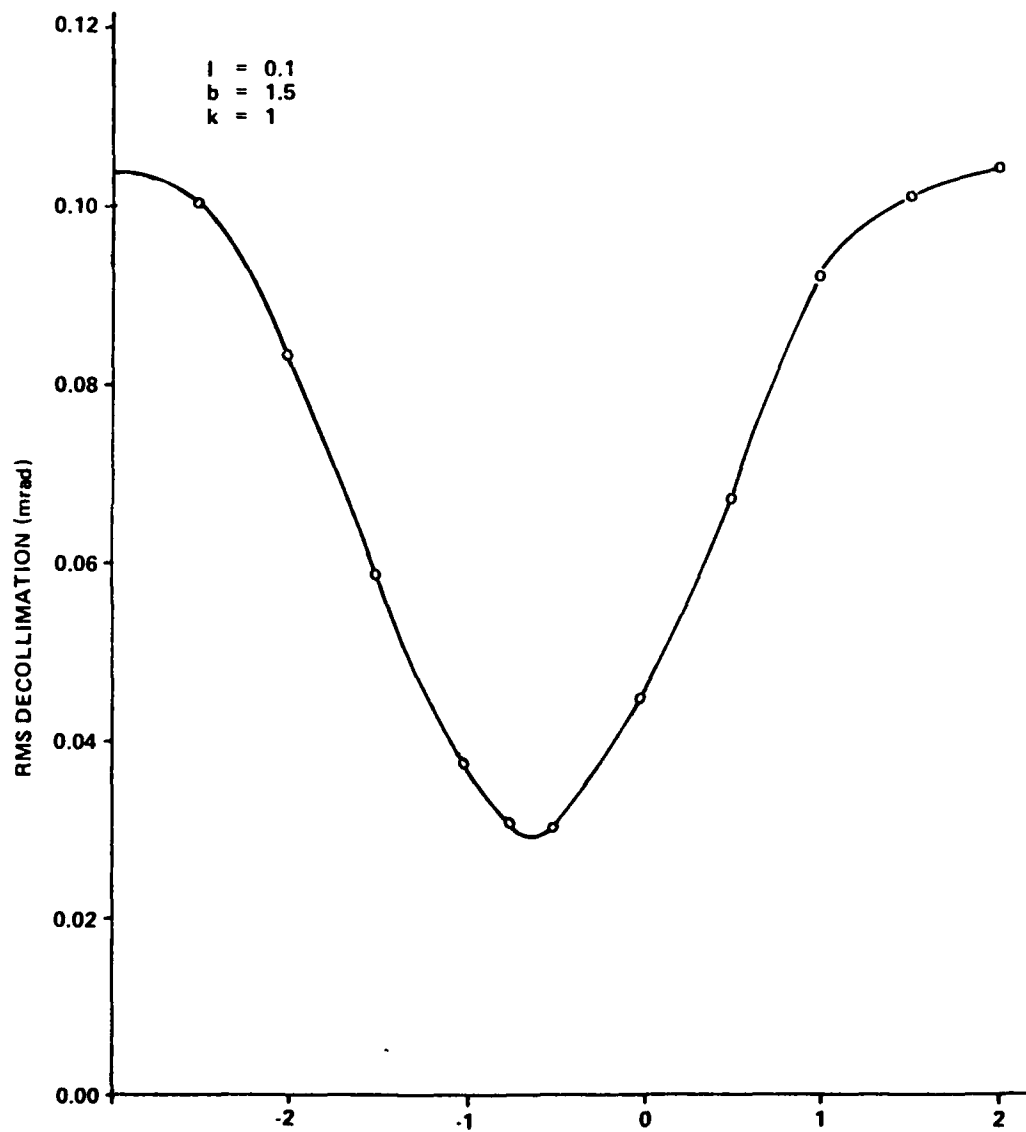


Figure 20. Sensitivity of decollimation to pivot-point of outer-mirror tilt (tilt angle = 0.1 mrad).

The effect of tilting the outer mirror can be best described by the nomogram in Figure 21. A straight-edge can be applied to this nomogram, and, for an arbitrary k , the rms decollimation produced by any tilt of the outer mirror can be seen immediately within the range of the nomogram.

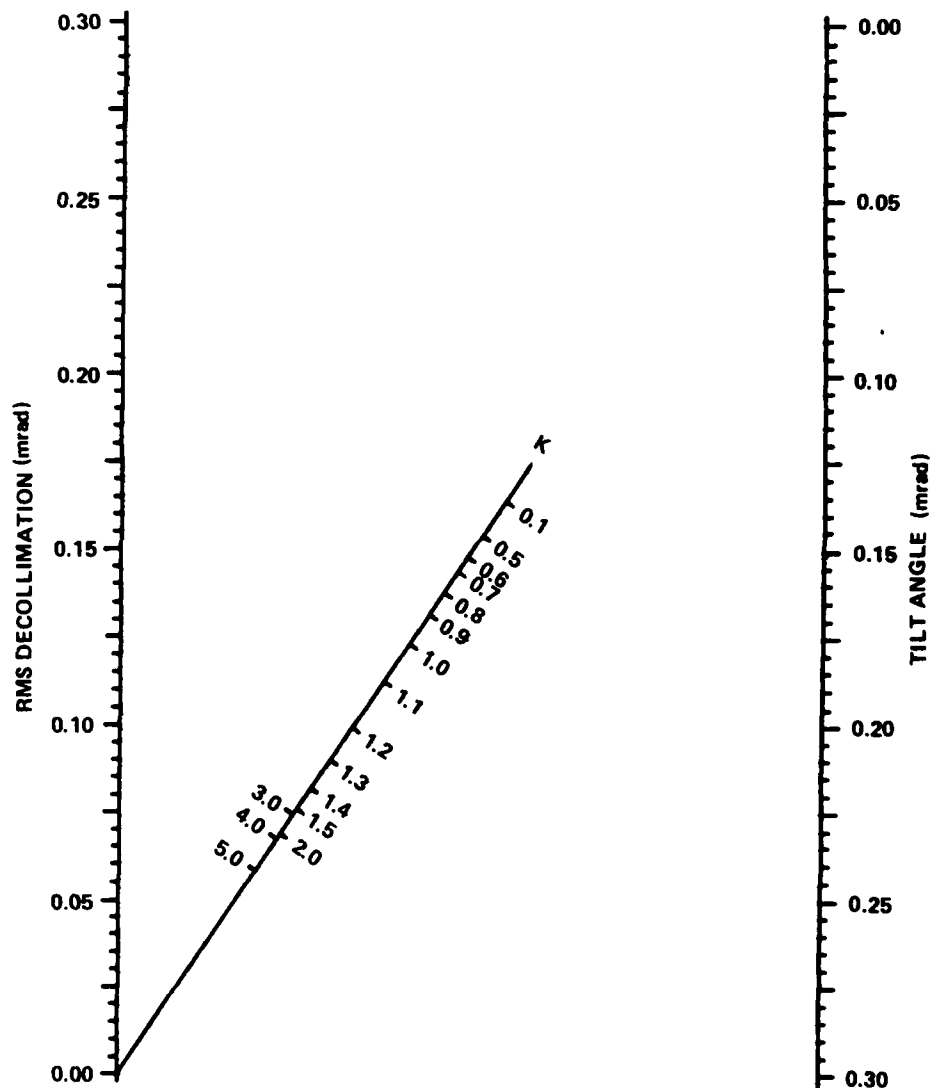


Figure 21. Nomogram relating beam decollimation, shape factor, and tilt of outer mirror.

Because of the slight dip in the curve relating decollimation to k , in the vicinity of $k = 2$, the k -scale folds back at $k = 2$ in the nomogram. The $k = 2$ case represents a system in which there is, roughly, a right-angle reflection at each mirror. The dip is not strong enough, though, to influence a decision in the choice of k significantly.

2. Decentering of the Outer Mirror

The beam degradation caused by decentering the outer mirror will now be considered. This is especially important because by usual alignment techniques, the centering of a component is usually much less precise than the angular alignment. Angular alignment can be readily accomplished with optical-tooling telescopes and interferometers. Centering, however, usually depends on aberration analysis because the optical center of an element may not coincide with the physical center. Diamond machined optics can be better in this respect, since the outside edge of the mirror can be machined in the same operation as the optical surface. This procedure would guarantee coincidence of the optical and geometrical centers. Depending on the configuration of the element and its mount, however, this may not always be feasible.

Figure 22 shows the variation of the decollimation with the decentering of the outer mirror for several k . Once again, it is noted that the variation is linear for any k . Thus, both tilt and decentering introduce coma.

The various k give different slopes to the straight lines, however, indicating a functional dependence of the decollimation on k , for any

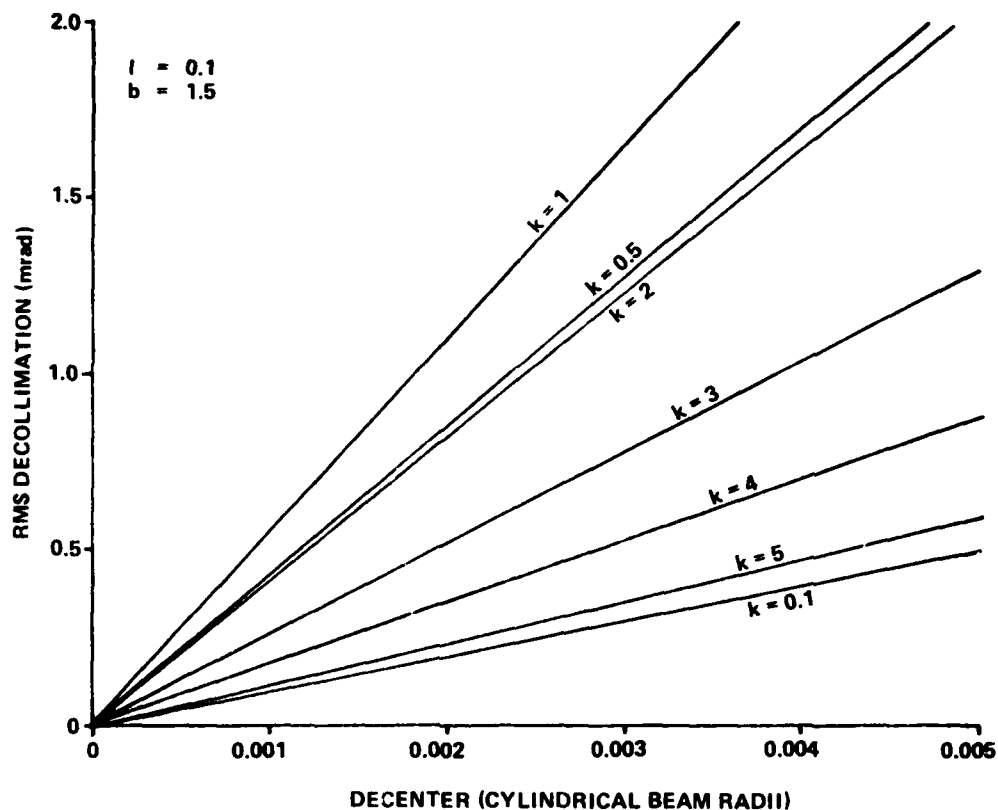


Figure 22. Beam decollimation versus decenter of outer mirror.

fixed amount of decentering. This dependence is shown in Figure 23, where the amount of decentering is taken as 0.002 times the input beam radius.

It should be noted that the grazing-incidence systems, $k = 0.1$, for example, show the least sensitivity to decentering, even though they are the most sensitive to tilt error. But even in these systems, the magnitude of the decollimation due to decentering is high compared to that produced by tilt. Near-normal-incidence systems ($k = 5$), have low sensitivity to both tilt and decentering.

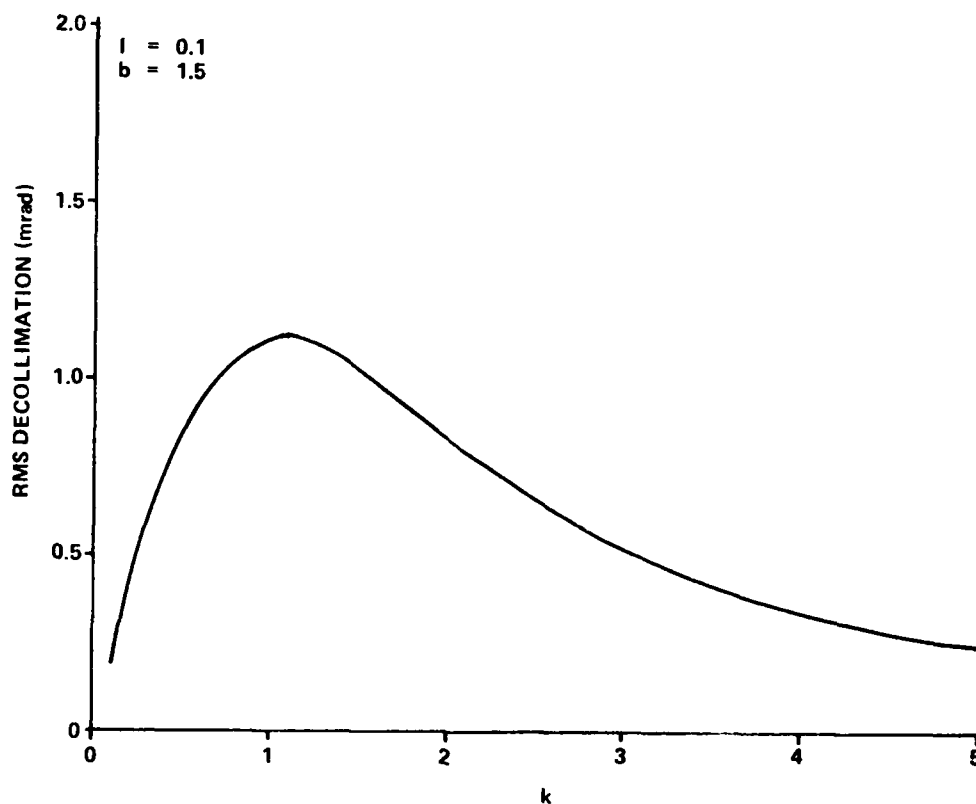


Figure 23. Beam decollimation versus shape factor for constant decenter of 0.002 cylindrical beam diameters at the outer mirror.

The most sensitive to decentering are intermediate systems such as those chosen in the example. From Figures 19 and 22, it can be seen that in the example in which $k = 1$, 0.1-mrad tilt produces approximately the same beam degradation as a decenter of 0.0015 times the input beam radius.

The effect of decentering the outer mirror can be determined quite easily from the nomogram in Figure 24. This nomogram is also read by

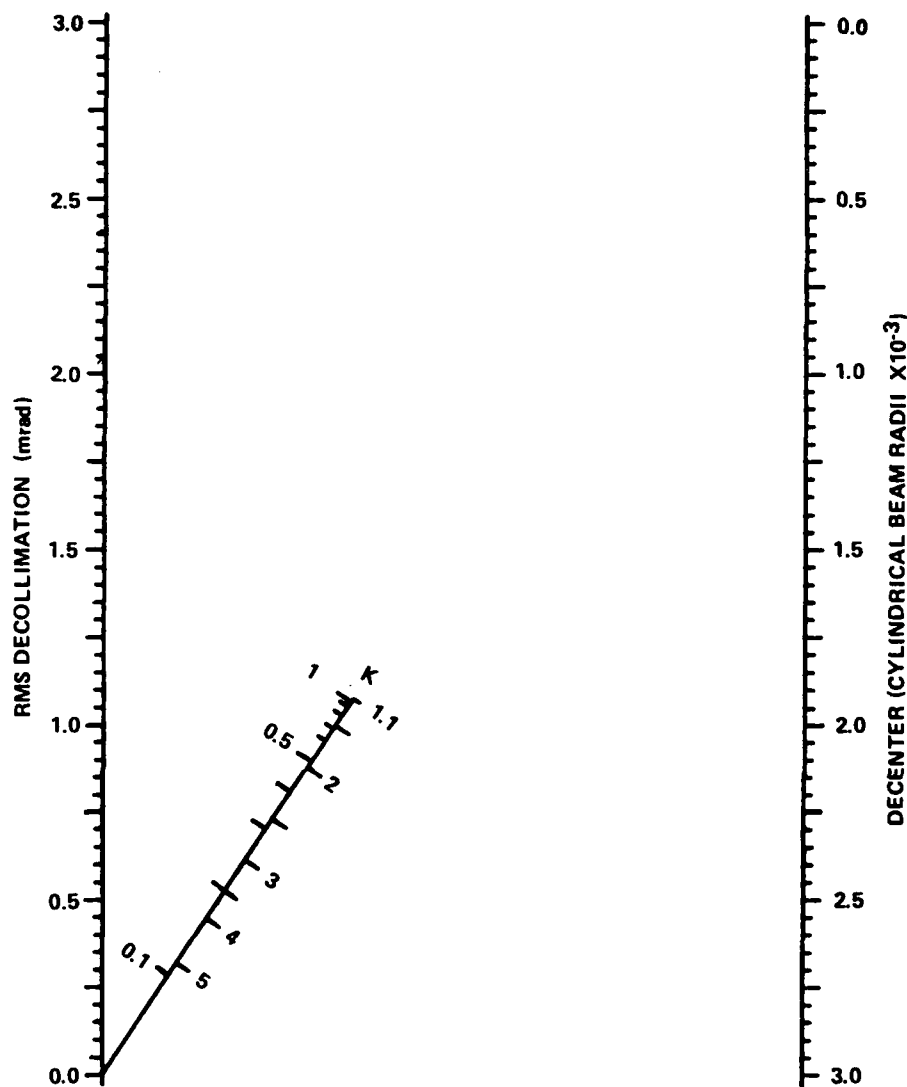


Figure 24. Nomogram relating beam decollimation, shape factor, and decentering outer mirror.

applying a straight-edge, and observing its intersections with the three scales.

The centroid shift resulting from a decentering of 0.002 input-beam radii is shown as a function of k , in Figure 25. Once again the grazing-incidence systems are least sensitive.

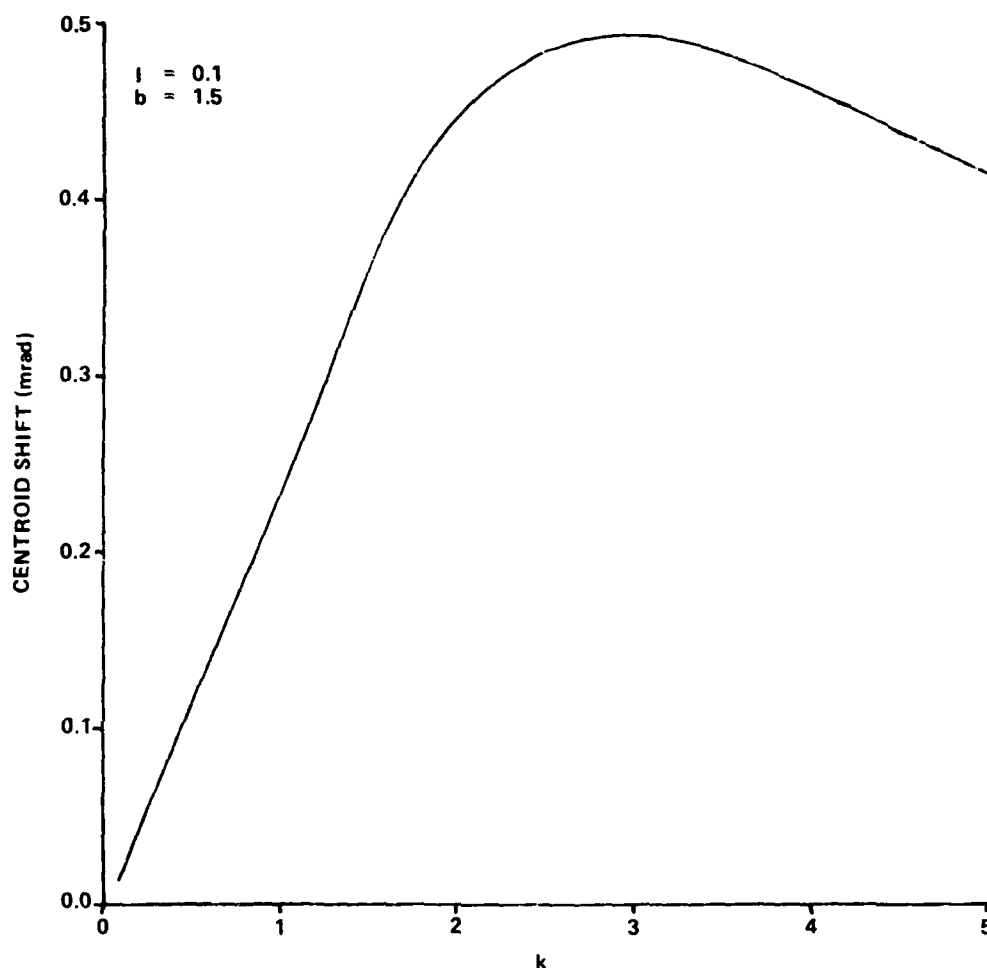


Figure 25. Centroid shift versus shape factor for constant decenter of 0.002 cylindrical beam diameters at the outer mirror.

The centroid shift is probably the least serious of all the effects of misalignment. In the laser systems in which a reflexicon might be used, this effect could be compensated by the aiming of the system. The system would simply be aimed to position the average beam spot center on the target. In some systems, this is done via an automatic hot-spot sensing system.

3. Despacing

It is obvious from Figure 26, that the reflexicon system is exceedingly sensitive to a mirror spacing error. In order to maintain an rms decollimation of not more than 0.1 mrad, the mirror spacing must be accurate to within 0.000017 times the input beam radius. If precise collimation of the output beam is required, the mirror spacing must be set with as high a precision as possible. Fortunately, this spacing can be readily checked by autocollimation.

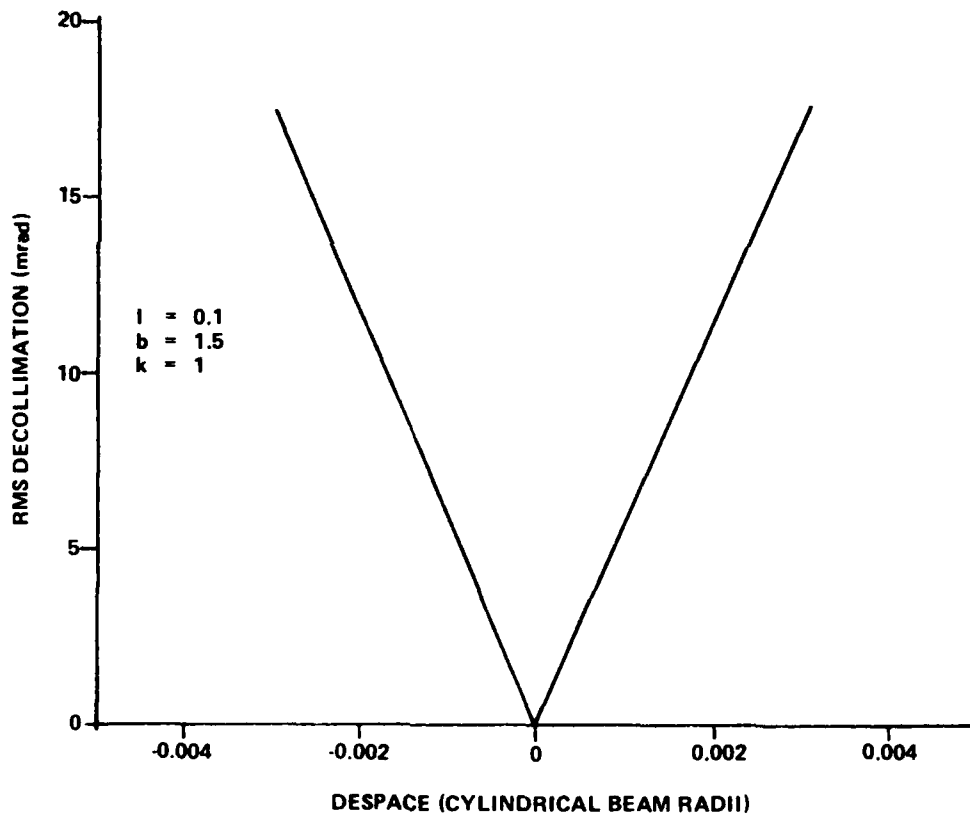


Figure 26. Beam decollimation versus despacing of mirrors.

4. Off-Axis Angle

When the reflexicon systems were checked for sensitivity to a misalignment of the whole system with respect to the input beam, it was found that the rms decollimation was independent of k , to within the error of computation (approximately seven significant figures). Thus, the graph in Figure 27 applies to all shape factors, at least within the range of $0.1 \leq k \leq 5$.

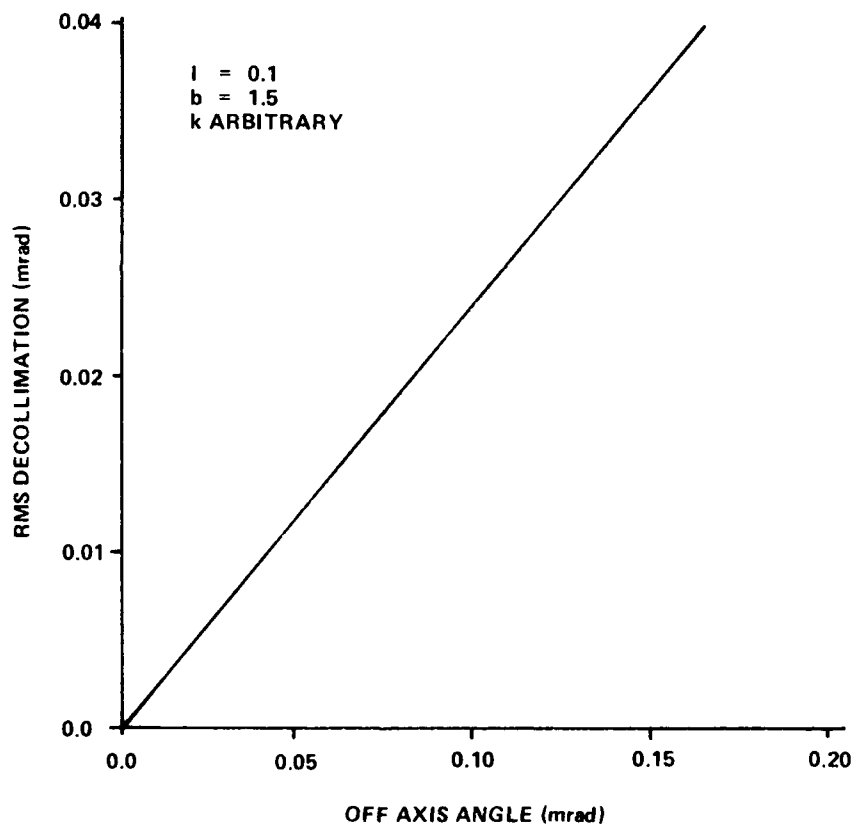


Figure 27. Beam decollimation versus off-axis angle of incident cylindrical beam.

The rms decollimation varies linearly with the off-axis angle, and is 0.245 times the off-axis angle in the example.

5. Inside Radius of Annular Beam

Thus far, annular beams having an inside radius of $\sqrt{1.5}$, or $b = 1.5$ have been considered. Although this parameter will usually be fixed by the size and type laser and/or optical system with which the reflaxicon is used, it is instructive to let b vary in the hypothetical system. Keeping k and I fixed at 1 and 0.1, respectively, and a tilt of 0.1 mrad at the outer mirror, the relationship between b and the rms beam decollimation can be found (Figure 28). The sensitivity to tilt increases with the inner radius of the annular beam. In order to minimize sensitivity to tilt, the inside radius of the annular beam should be kept as close to the outside radius of the cylindrical beam as possible.

Figure 29 shows the relationship between decollimation and b when the outer mirror is decentered by 0.002 times the input beam radius. The effect is just the reverse of the tilt sensitivity. The larger the inside radius of the annular beam, the less sensitive the system is to decentering.

6. Intensity Transformation

The intensity transformation function will almost certainly be determined by factors other than alignment sensitivity. However, Figure 30 shows beam decollimation for a range of intensity transformations with a constant tilt of 0.1 mrad. The model system becomes very sensitive to tilt when the intensity transformation becomes very small

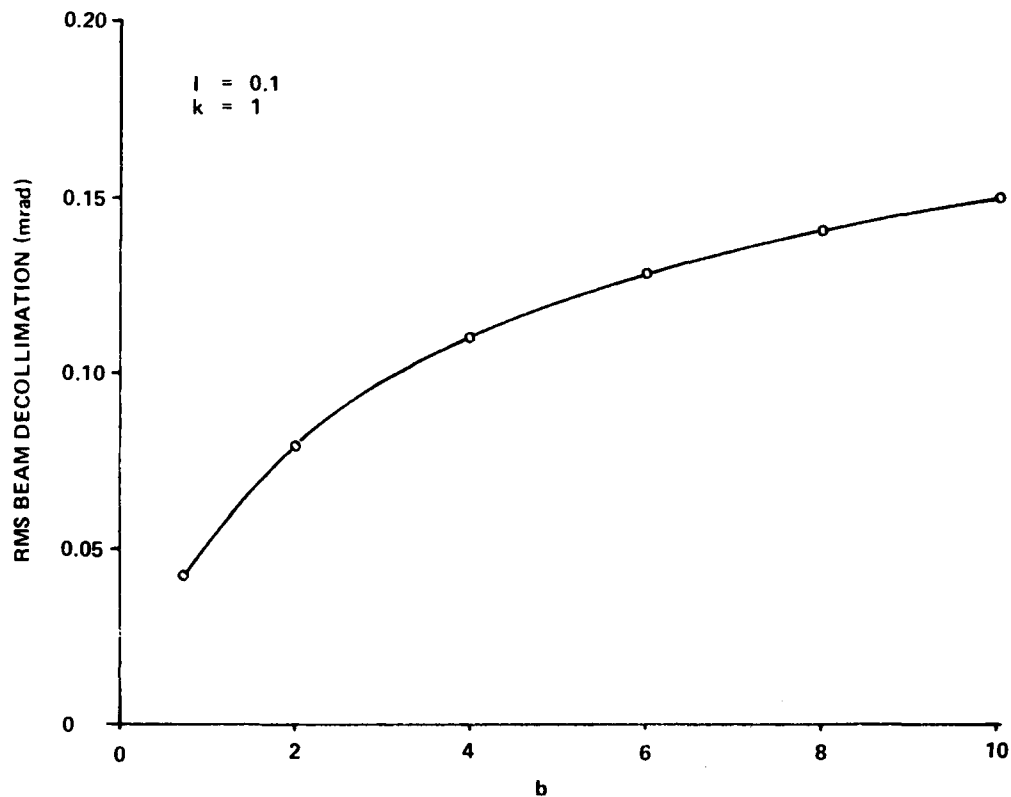


Figure 28. Beam decollimation versus inside radius of annular beam for constant tilt of 0.1 mrad at outer mirror.

or large. The chosen value of $I \approx 0.1$ is nearly optimum for this system. Figure 31 is similar, but for a constant decentering of 0.002 input-beam radii.

7. Statistical Analysis

Obviously, there are many factors which govern the performance of a reflaxicon, some of which have opposing effects. At this point, all angular and linear misalignments will be allowed to occur simultaneously. The angular misalignments were varied

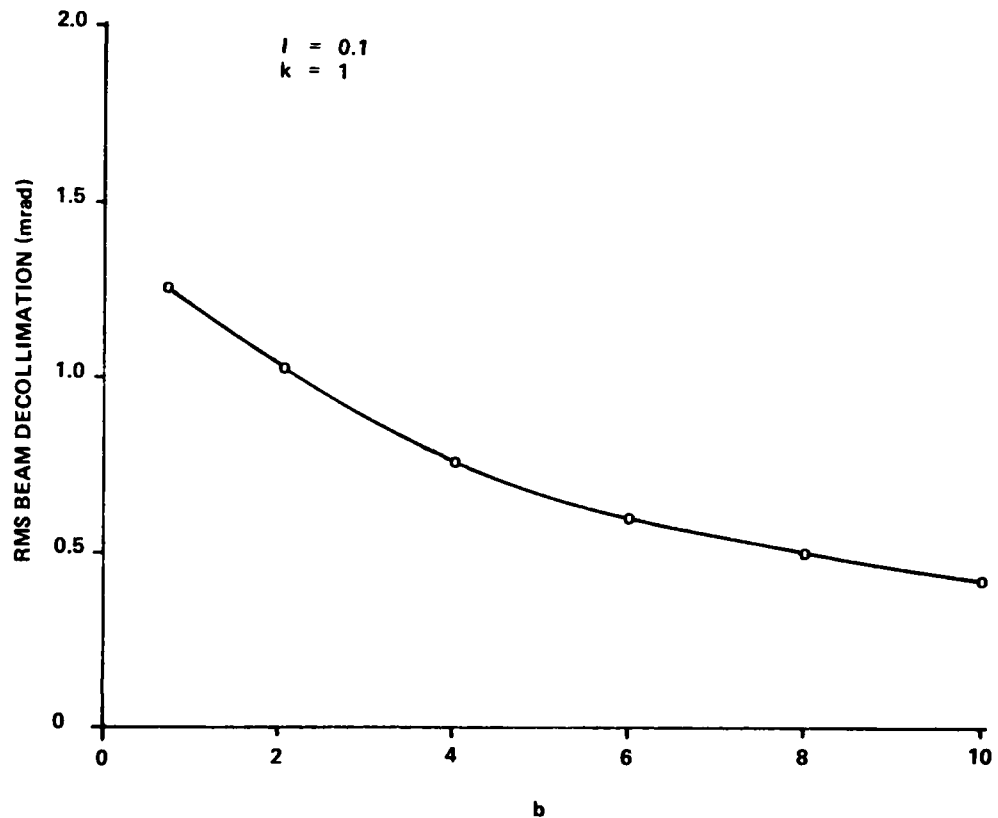


Figure 29. Beam decollimation versus inside radius of annular beam for constant decenter of 0.002 cylindrical beam diameters at outer mirror.

within a range of ± 0.1 mrad, and the linear errors varied randomly within a range of 0.001 times the radius of the cylindrical input beam. This was accomplished by multiplying each error limit by a random number between 1 and -1. The system was ray-traced 100 times, using 112 rays per run. The shape-factor was varied through the range from $k = 0.1$ to $k = 5$.

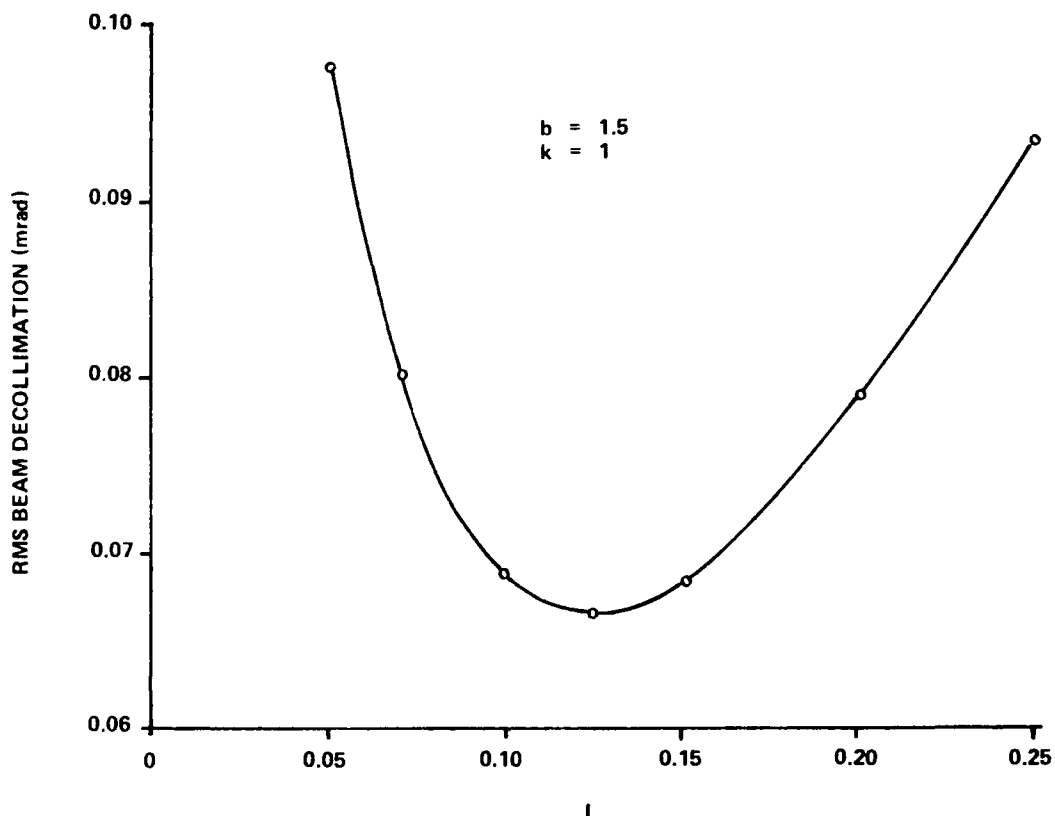


Figure 30. Beam decollimation versus intensity transformation for constant tilt of 0.1 mrad at outer mirror.

Figure 32 shows the results of these calculations. The mean values of the rms decollimations are plotted along with the standard deviations. It can be seen that the decentering was the dominant error, since Figure 32 looks very much like Figure 23.

The standard deviations are rather large, but making 200 sets of calculations per data point, instead of 100, produced almost no change in the standard deviation of the mean rms decollimation. The mean value of the rms decollimations was repeatable within 5%.

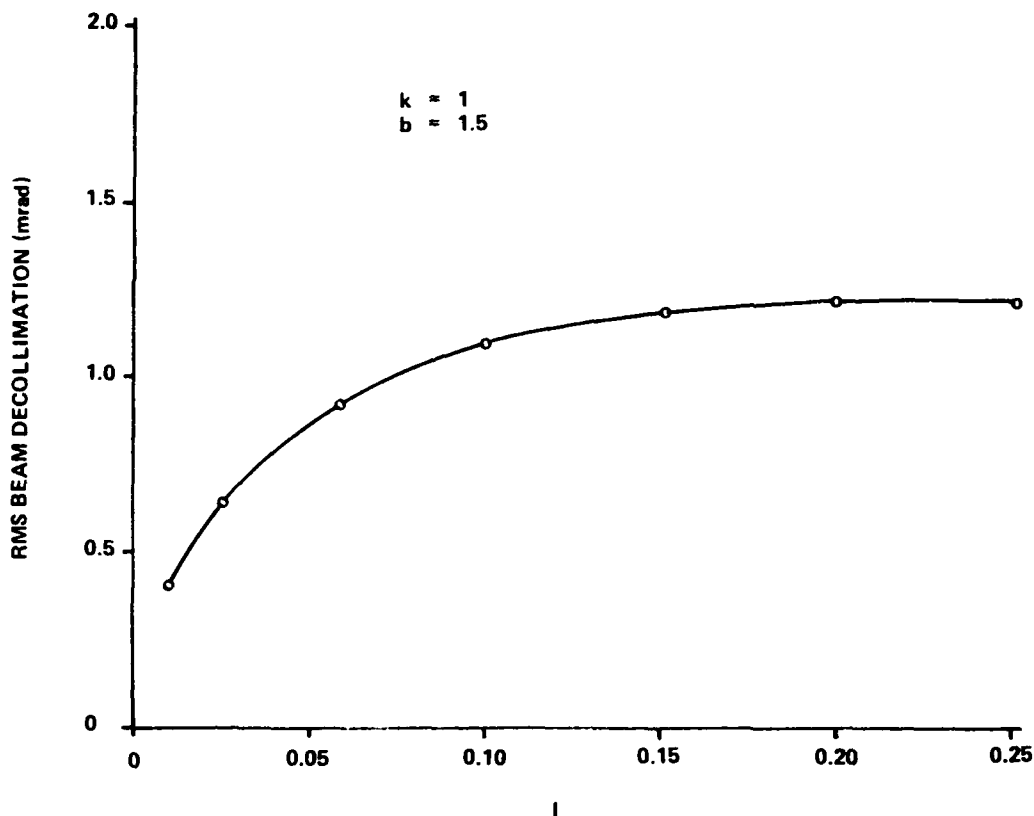


Figure 31. Beam decollimation versus intensity transformation for constant decenter of 0.002 cylindrical beam diameters at outer mirror.

Figures 33 through 39 show the distributions for each plotted value of k . They show the percentage of runs falling within 0.1-mrad increments of decollimation. It is noted that the narrowest distribution and the best performance were given by the grazing-incidence system, $k = 0.1$.

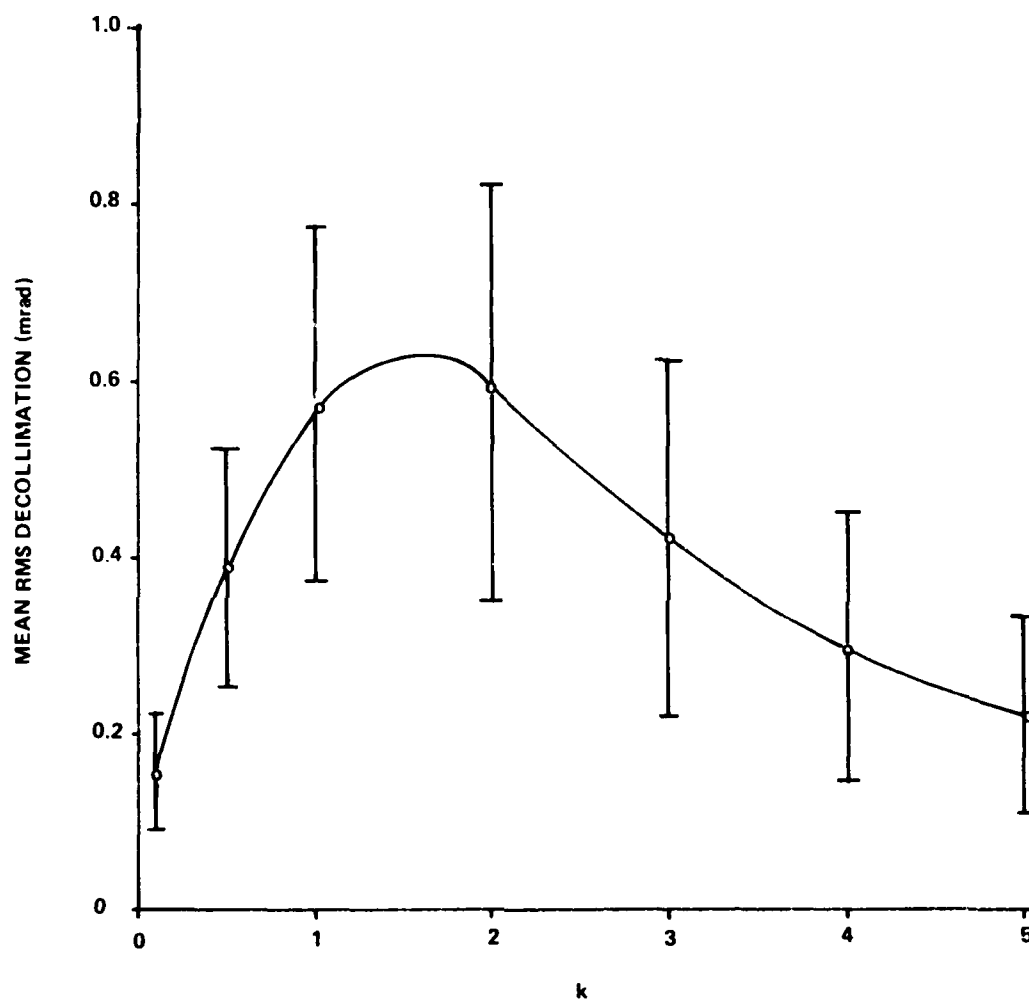


Figure 32. Statistical beam decollimation versus shape factor for tilt limits of 0.1 mrad and shift limits of 0.001 cylindrical beam diameter with standard deviations.

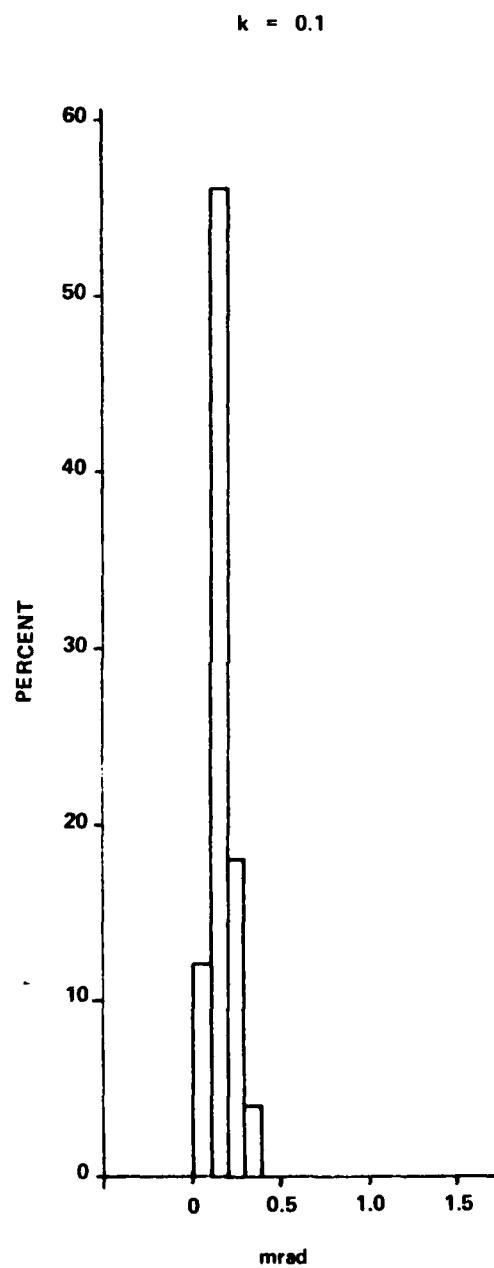


Figure 33. Decollimation distribution, $k = 0.1$.

$k = 0.5$

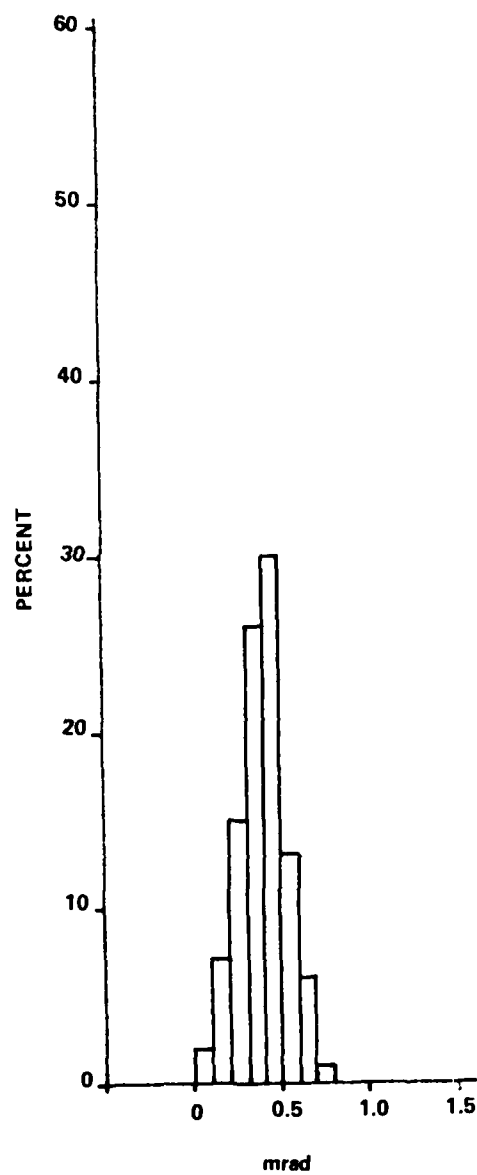


Figure 34. Decollimation distribution, $k = 0.5$.

$k = 1$

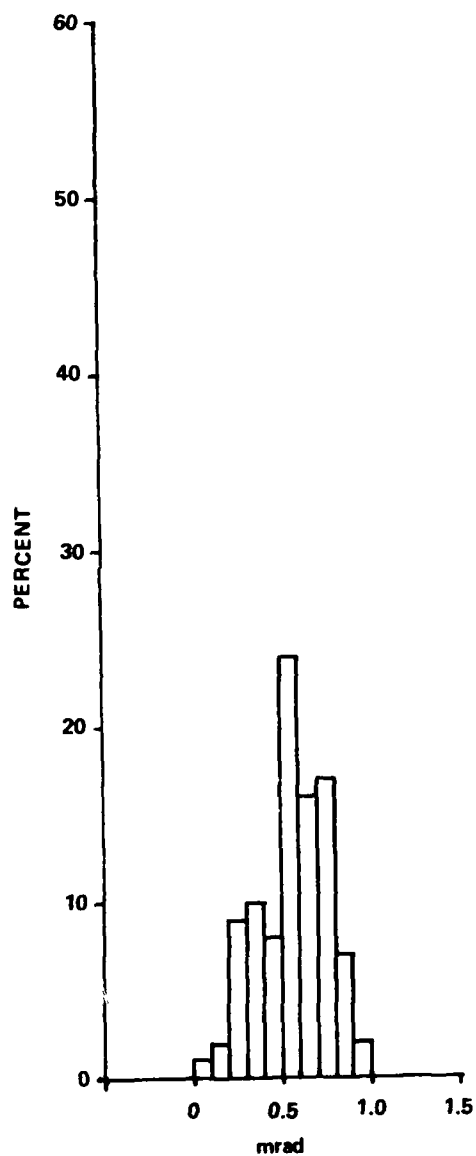


Figure 35. Decollimation distribution, $k = 1$.

$k = 2$

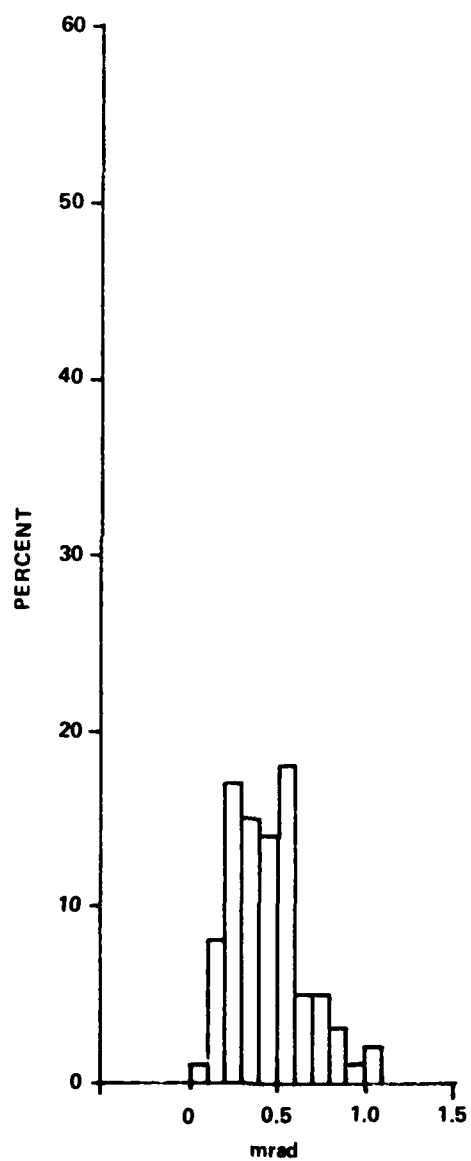


Figure 36. Decollimation distribution, $k = 2$.

$k = 3$

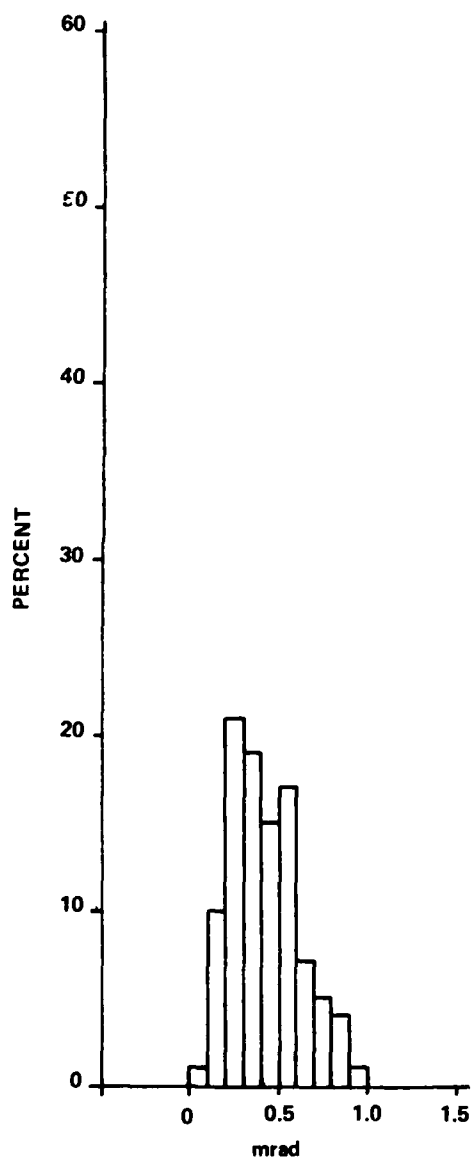


Figure 37. Decollimation distribution, $k = 3$.

$k = 4$

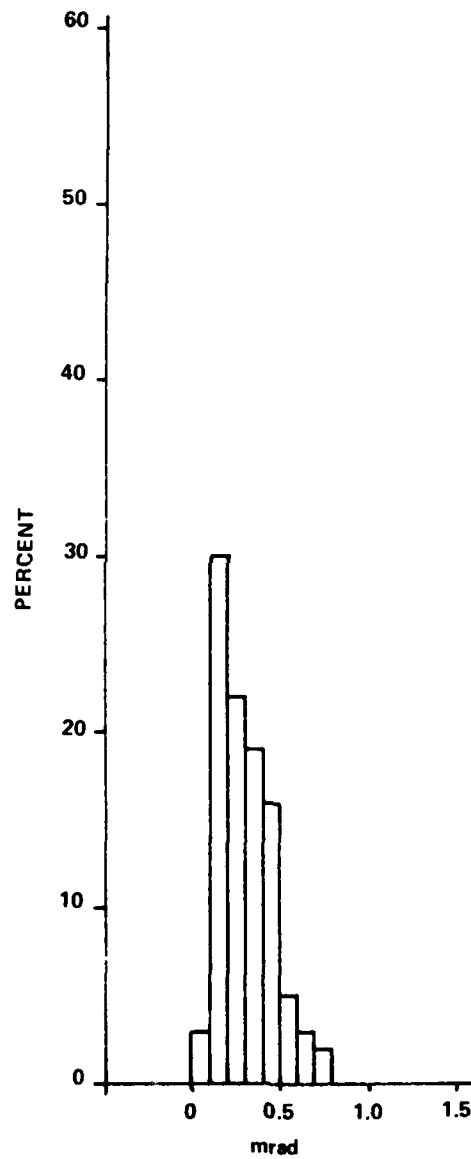


Figure 38. Decollimation distribution, $k = 4$.

$k = 5$

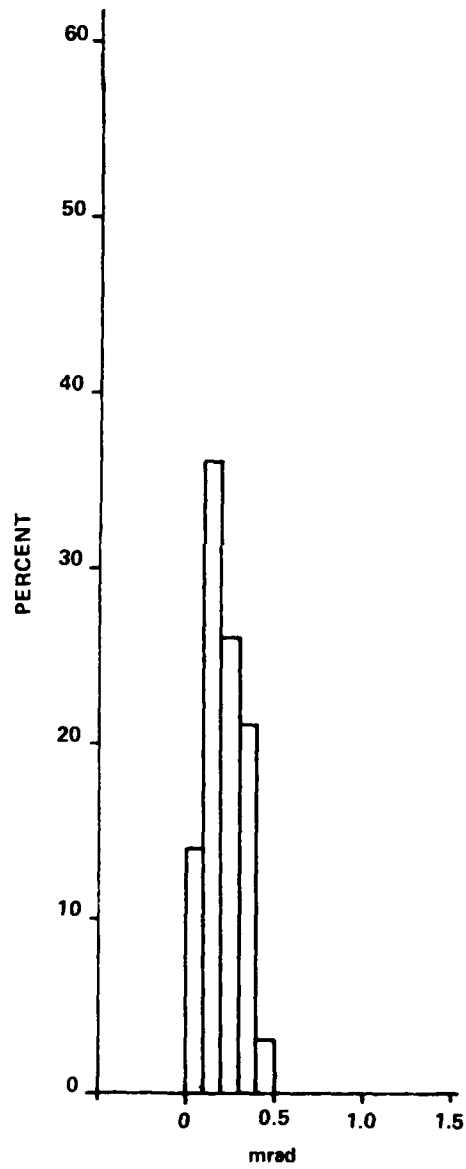


Figure 39. Decollimation distribution, $k = 5$.

C. Waxicon Systems

Waxicons, as they are commonly constructed, present far fewer alignment problems than reflaxicons. A waxicon system is almost always made in one piece with both mirrors machined on a single metal blank. This would not be practical with a reflaxicon system because the beam must pass through the system. The support structure for the inner mirror would interfere with the machining of the outer mirror, and the two mirrors face opposite directions, requiring that the blank be removed from the lathe and turned around to machine the other side. Proper alignment would be very difficult to preserve in this way.

Since waxicons can be machined from one piece of metal, this procedure should always be followed unless extraordinary design constraints prohibit it. If the two mirrors are machined on a single blank without removing the blank from the lathe until the work is completed, there will not be any significant alignment error within the system. The centering and the angular alignment will be as good as, and probably better than, the figure accuracy of the surfaces. This can certainly be within fractional wavelength tolerances. The spacing of the mirrors will have roughly the same accuracy and precision as the mirror surfaces. Thus, the only realistic alignment error is a misalignment of the entire waxicon with the input beam. If the system is used with a collimated beam, there is zero sensitivity to a lateral displacement of the system, leaving only an off-axis tilt as the only source of alignment error.

Even though the waxicon would almost always be made in one piece, nevertheless, the sensitivity of the outer mirror to decenter and tilt will be examined.

A model system will be defined just as it was for the reflaxicon. In this case, the intensity transformation, $I = 0.1$, will be retained and the outside radius of the annular beam will be $\sqrt{b} = 4$. The constant, C , will be allowed to vary at will.

1. Decentering

Following exactly the same procedures that were used with the reflaxicon, and remembering that the waxicon shape-factor is the constant C , a decenter of 0.001 input-beam radii on the outer mirror will be imposed and the rms decollimation as a function of C will be observed. This relationship is shown in Figure 40. The first thing noticed in this graph is that the magnitude of the decollimation is much larger than that in the reflaxicon. Also, by far the best performance is with a small C . Such a system would have near-grazing-incidence of the inner mirror and almost normal-incidence on the outer mirror.

If C is held constant, and the amount of decenter varied, Figure 41 shows that the variation in decollimation is linear, just as it was in the reflaxicon.

Combining the results of Figures 40 and 41, a nomogram can be constructed for arbitrary shifts and shape-factors, as shown in Figure 42. A straight-edge is used with this nomogram in the same fashion as with the reflaxicon nomograms.

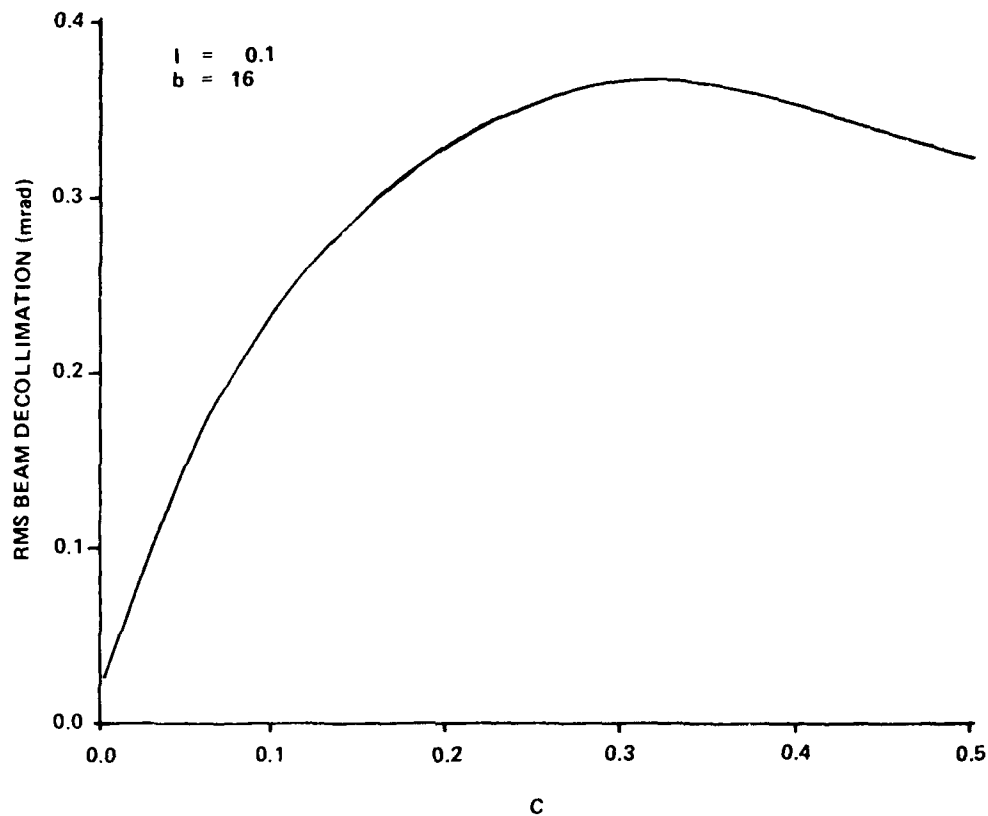


Figure 40. Beam decollimation versus shape factor for constant decenter of 0.001 cylindrical beam diameters at outer mirror.

2. Tilt in the Waxicon

If the tilt of the outer mirror is held constant and the shape-factor allowed to vary, the variation in decollimation is shown in Figure 43.

Once again, the system with a small C performs far better than those with large C , and is comparable in performance to the reflaxicons. A large C makes the waxicon very sensitive to mirror tilt.

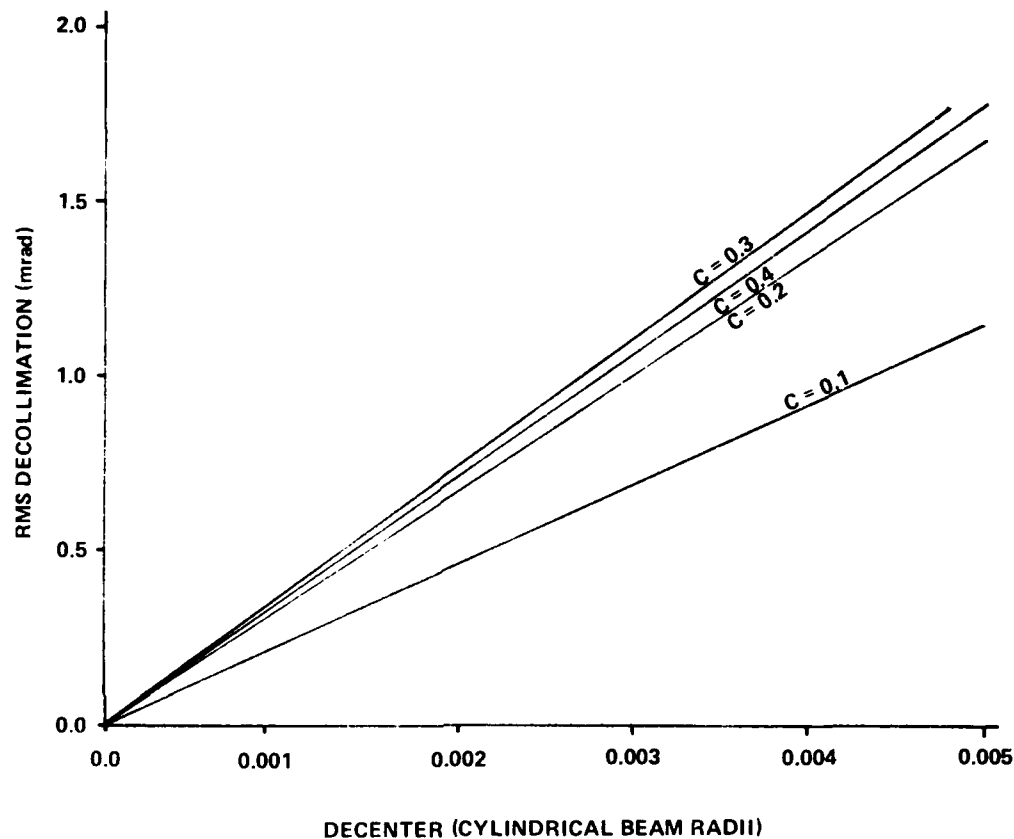


Figure 41. Beam decollimation versus decenter of outer mirror for constant C .

If C is held constant, and the tilt-angle allowed to change, the familiar linear relationship between tilt and decollimation results as shown in Figure 44.

Combining the information in Figures 43 and 44, the decollimation can be shown resulting from an arbitrary tilt and arbitrary C . A nomogram showing this is given in Figure 45. It is also read with a straight-edge.

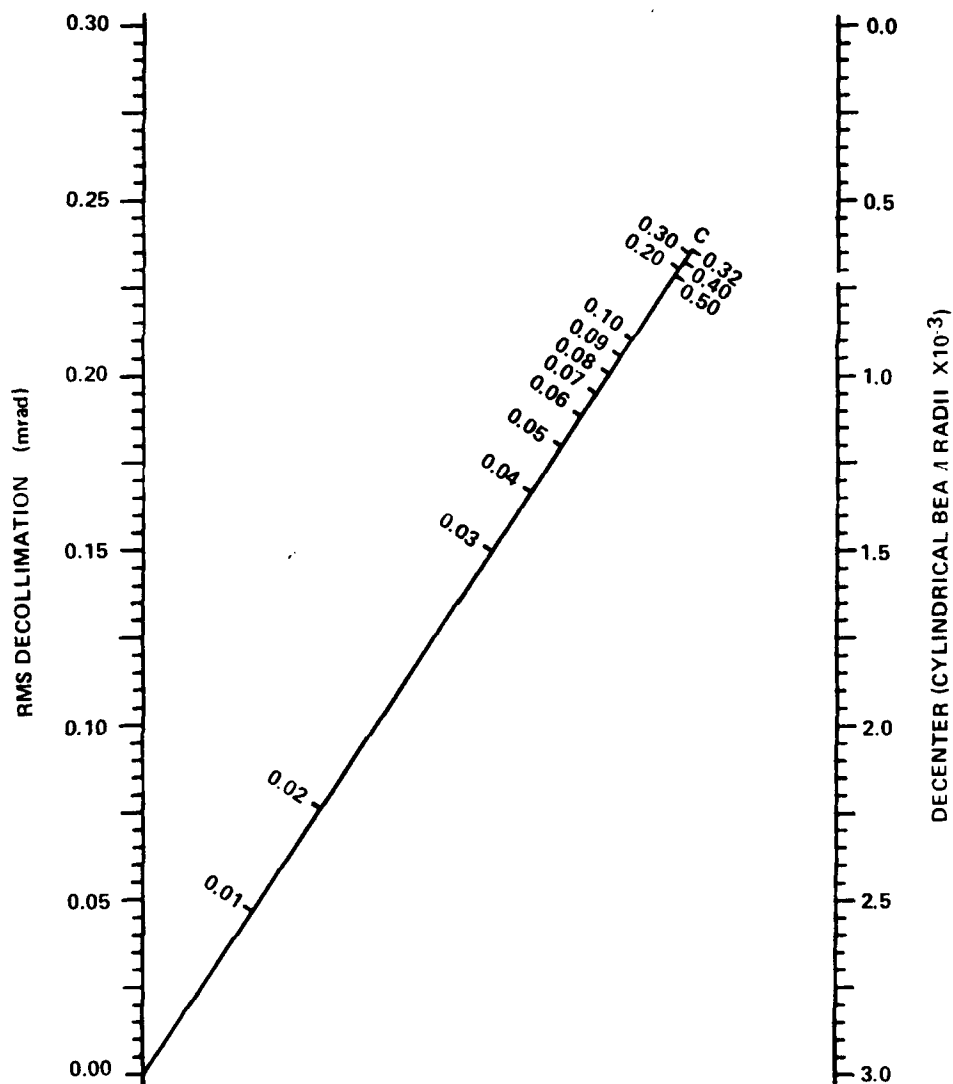


Figure 42. Nomogram relating beam decollimation, shape factor, and decentering of outer mirror.

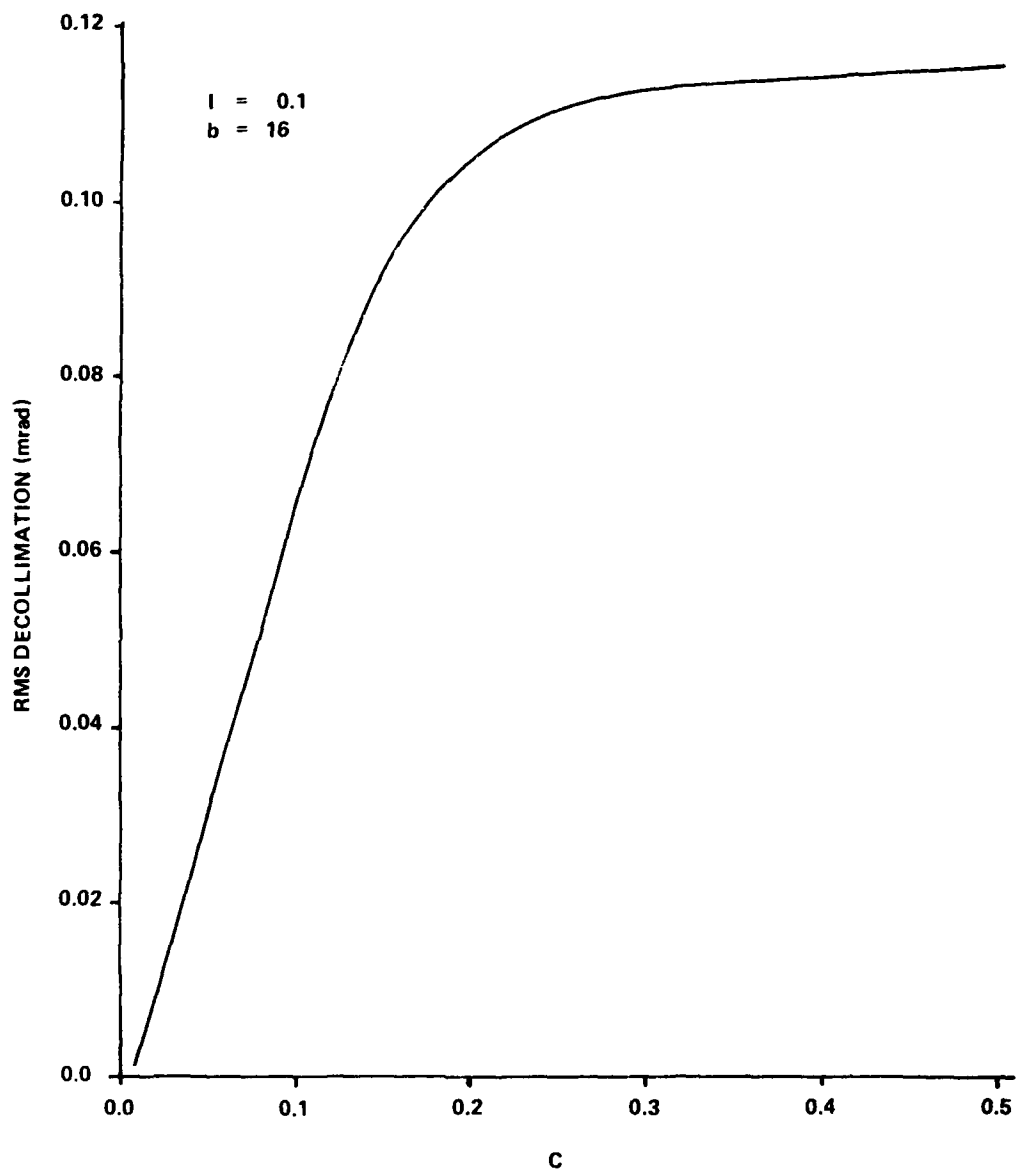


Figure 43. Beam decollimation versus shape factor for constant outer mirror tilt of 0.1 mrad.

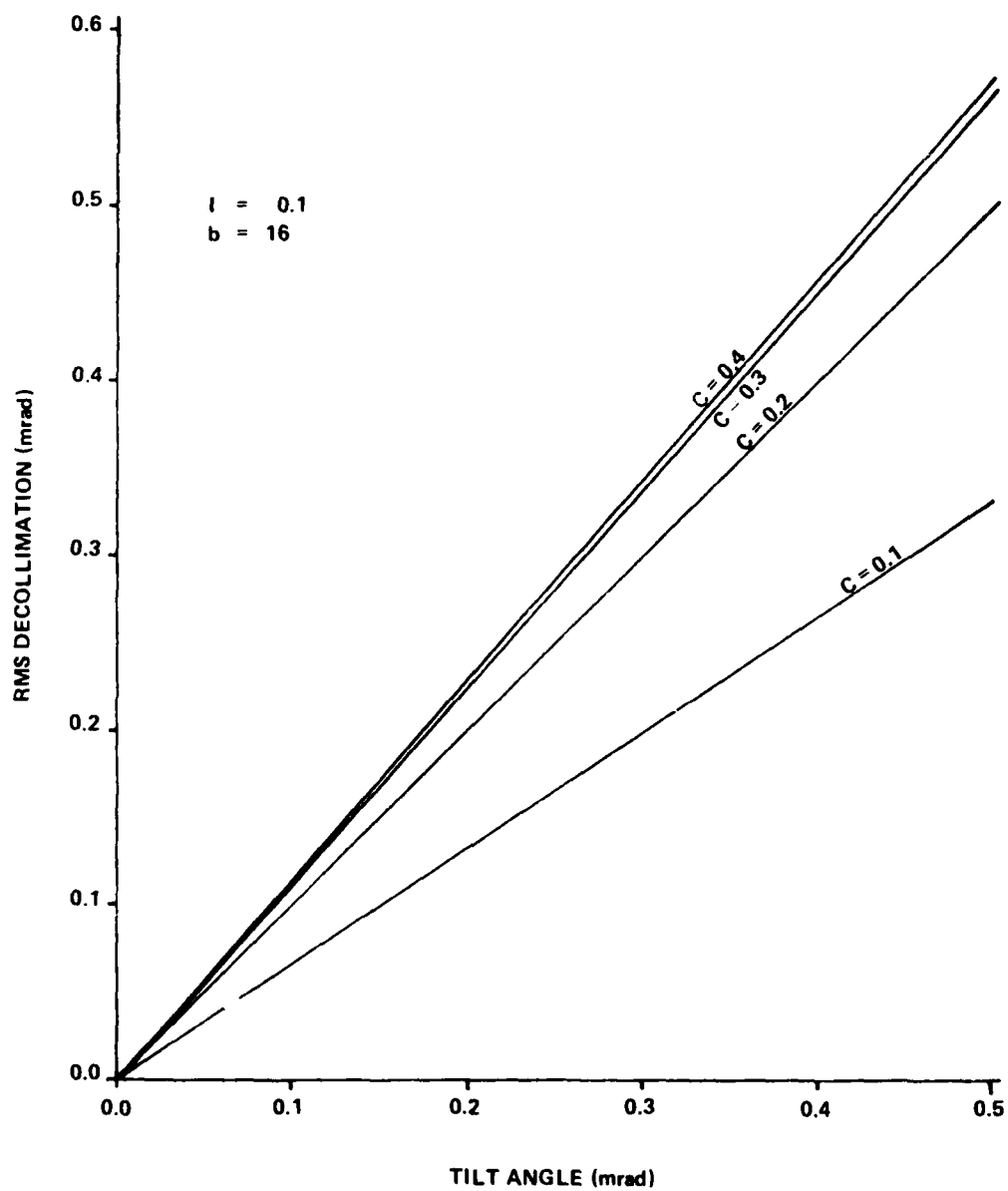


Figure 44. Beam decollimation versus tilt of outer mirror.

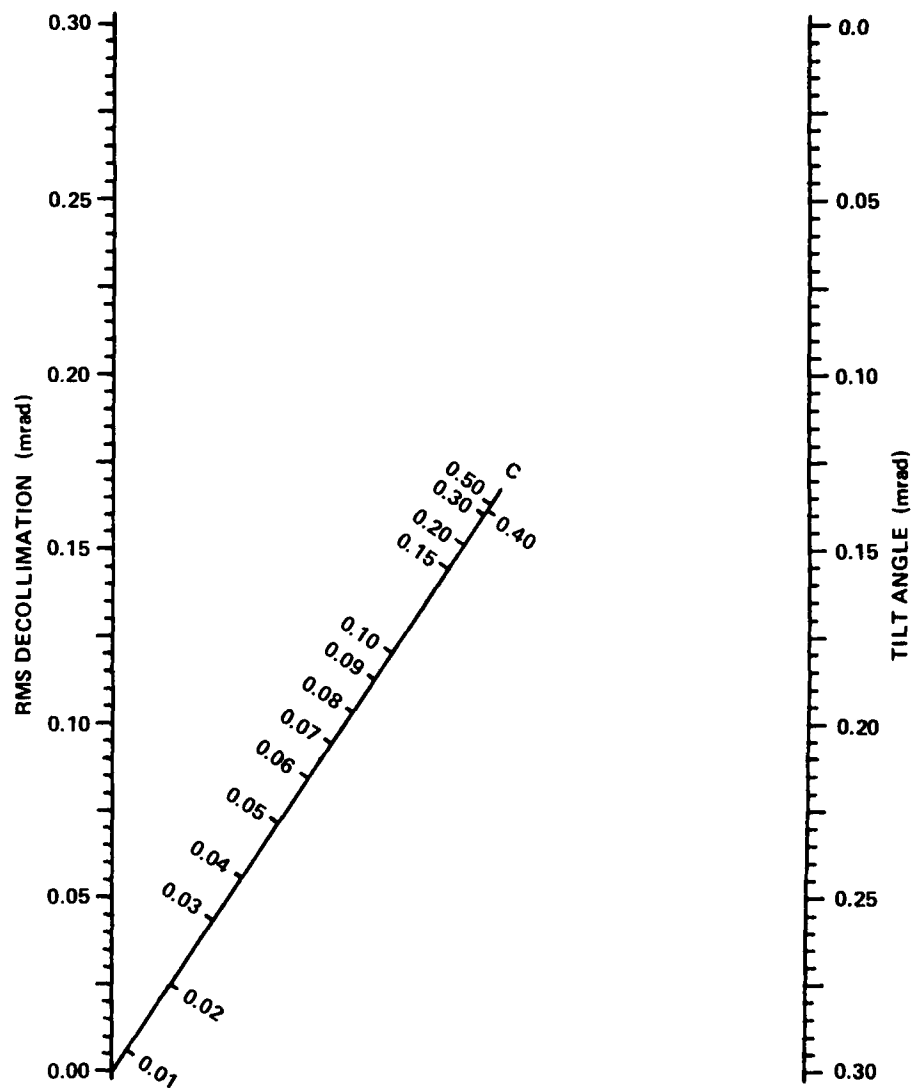


Figure 45. Nomogram relating beam decollimation, shape factor, and tilt angle.

3. Off-Axis Angle

This is the only misalignment that is usually meaningful. It is, therefore, of particular interest. If the decollimation is computed as a function of the off-axis angle for many values of C , it is found to be independent of C . This is the same phenomenon found in the reflexicon system. Figure 46 shows the rms decollimation to be equal to 1.21 times the off-axis angle.

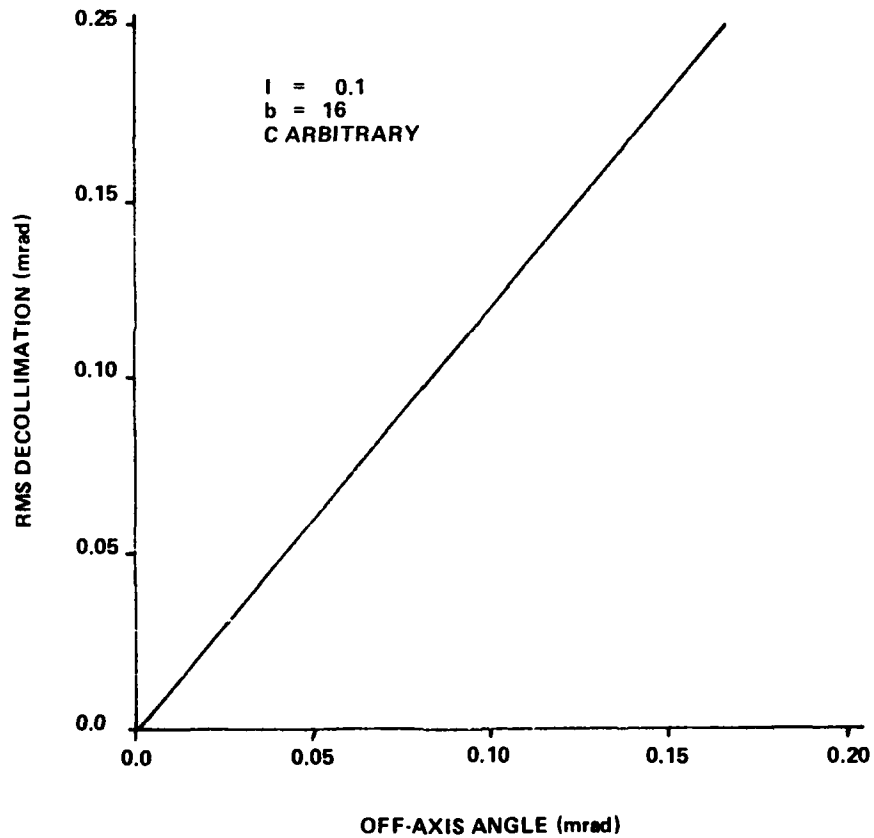


Figure 46. Beam decollimation versus off-axis angle of incident cylindrical beam.

The rms decollimation was calculated for 100 off-axis tilt angles, randomly chosen between the limits of -0.1 and $+0.1$ mrad. The mean of the rms decollimations was found to be 0.053 mrad with a standard deviation of 0.031 mrad. This is less than half the decollimation found in the statistical analysis of the best reflexicon ($k = 0.1$) with its many sources of appreciable error.

Chapter V. CONCLUSIONS

Reflaxicons and waxicons are extremely versatile systems, capable of performing ray-height and intensity transformations that could not be achieved with classical optical systems. The mathematical theory has been developed for completely generalized transformations in two-mirror, afocal systems.

It has been shown that near-grazing-incidence reflaxicons are capable of better performance than the more common configurations because they are more tolerant of misalignment.

Waxicons are to be preferred to reflaxicons, whenever this configuration is feasible. Their primary advantage is that they can be made in one piece, thereby eliminating most of the potential sources of misalignment.

The preferred configuration for waxicons is that with a small shape-factor. This configuration is not likely to cause serious polarization problems when used with dielectric coatings. The inner mirror, which usually has the higher heat-loading, is used at almost grazing incidence. This spreads the heat load over a larger area and improves the reflectivity. It is a convenient configuration for diamond-machining. This is a very different configuration from that which is usually produced.

Waxicons are usually restricted to applications in which retro-reflection is required, but they could readily be used as fixed-focus, telescopic systems if combined with a flat mirror to turn one of the beams to the side. If this flat is an annular mirror reflecting the annular beam, there would be no need to have a mirror support structure obstructing either the input or the output beams. The system would be completely unobstructed.

In view of the high performance of afocal waxicons, it is recommended that focusing waxicons be systematically studied to determine their suitability for use in laser welding and cutting devices. They would allow contouring of the beam intensity profile to optimize the welding and cutting processes and would probably be less sensitive to alignment errors than more conventional focusing systems. Thus far, their use in this field has been almost completely ignored.

There is also a great need for beam-contouring reflaxicons which can be focused over a reasonable range. These systems would have to use more than two mirrors. They would be particularly useful in pointing and tracking systems for high-energy lasers.

SELECTED BIBLIOGRAPHY

Periodicals

- Arnold, J. B., Sladky, R. E., Steger, P. J., and Woodall, N. D., "Machining Nonconventional-Shaped Optics," Optical Engineering, Vol. 16, July-August 1977, pp. 347-354.
- Bakken, George S., "The Parabolic Axicon," Applied Optics, Vol. 13, June 1974, pp. 1291-1292.
- Banks, D. S., "Toric Catoptrics," Electronic Progress, Vol. 17, Summer 1974, pp. 13-19.
- Fink, David, "Polarization Effects of Axicons," Applied Optics, March 1979, p. 581.
- Lavoie, Louis, "Conical Axicons Used as Optical Polar Everters," Applied Optics, Vol. 14, July 1975, pp. 1482-1484.
- Mansell, Dennis N., and Saito, Theodore T., "Design and Fabrication of a Nonlinear Waxicon," Optical Engineering, Vol. 16, July-August 1977, pp. 355-359.
- Ogland, J. W., "Mirror System for Uniform Beam Transformation In High-Power Annular Lasers," Applied Optics, Vol. 17, September 1978, pp. 2917-2923.
- Popov, L. V., "Fabrication of Optical Components by Diamond Turning," Soviet Journal of Optical Technology, Vol. 45(10), October 1978, pp. 648-650.
- Sakayanagi, Y., and Aoki, S., "Soft X-Ray Imaging With Toroidal Mirrors," Applied Optics, Vol. 17, February 1978, pp. 601-603.

Patents

- Rambauske, Werner R., "Catoptric Lens Arrangement," US Patent 3,827,059, July 30, 1974.

Reports

Korsch, Dietrich, Ray-Trace Evaluation Program, Teledyne Brown
Engineering, Huntsville, Alabama, 1977.

DISTRIBUTION

	<u>No. of Copies</u>
DRSM1-LP, Mr. Voigt	1
-R	1
-RH	1
-RHB	10
-RPR	15
-RPT (Record Copy)	1
(Reference Copy)	1

END 2-81